



HAL
open science

Recent developments in nuclear heating measurement methods inside the OSIRIS reactor

Hubert Carcreff, Laurent Salmon, Fadhel Malouch

► **To cite this version:**

Hubert Carcreff, Laurent Salmon, Fadhel Malouch. Recent developments in nuclear heating measurement methods inside the OSIRIS reactor. Nuclear Instruments and Methods in Physics Research Section A: Accelerators, Spectrometers, Detectors and Associated Equipment, 2019, 942, pp.162310. 10.1016/j.nima.2019.06.051 . cea-02535369

HAL Id: cea-02535369

<https://cea.hal.science/cea-02535369>

Submitted on 25 Oct 2021

HAL is a multi-disciplinary open access archive for the deposit and dissemination of scientific research documents, whether they are published or not. The documents may come from teaching and research institutions in France or abroad, or from public or private research centers.

L'archive ouverte pluridisciplinaire **HAL**, est destinée au dépôt et à la diffusion de documents scientifiques de niveau recherche, publiés ou non, émanant des établissements d'enseignement et de recherche français ou étrangers, des laboratoires publics ou privés.



Distributed under a Creative Commons Attribution - NonCommercial 4.0 International License

17 prototypes in various reactor conditions. A comparison is made with previous calorimeters and obtained advantages are
18 emphasized. This new calorimeter has been designed as a real operational measurement system, well suited to characterize the
19 radiation field inside an MTR reactor.

20

21 © 2001 Elsevier Science. All rights reserved

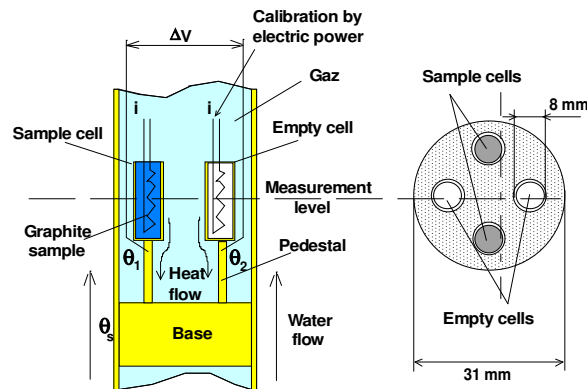
22 *Keywords* : Nuclear heating, differential calorimeter, incore measurements, OSIRIS reactor, mobile probe

23 **1. Introduction**

24 Nuclear heating inside an MTR reactor has to be known in order to predict sample temperatures during
25 irradiation experiments and for safety reasons, to demonstrate that the highest temperature inside irradiation
26 devices will not exceed material and thermohydraulic limits. Nuclear heating rate inside an MTR reactor is
27 usually done using calorimeters. A calorimetric measurement in reactors can be done either with a sensor
28 working in adiabatic mode (without heat exchange with the outside and measurement of temperatures in
29 evolution), or with a sensor working in permanent mode (heat exchange with outside and stabilized temperatures
30 in the sensor). Homemade calorimeters [1, 2, and 3], working in permanent mode, have been used for many years
31 for the qualification of irradiation locations in the pool type MTR OSIRIS reactor.

32 Until recent years, OSIRIS calorimeters were designed with a pair of two aluminum cells, fixed onto the same
33 aluminum base. Cells of each pair, both located at the same measurement level in the radiation field, are similar
34 except that one contains a graphite sample while the other one has the corresponding volume filled with nitrogen
35 (See Fig.1).

36



37

38 Fig.1. Static differential calorimeter previously used for heating measurements inside the OSIRIS reactor.

39 The two pairs of cells are diametrically opposed on the aluminum base to avoid any gradient effect in the
 40 calorimeter (heating radial distribution in the reactor). The whole structure is enclosed inside a tube in contact
 41 with the external water flow for heat removal. The pedestal, between the upper part of the cell and the base in
 42 contact with the external sleeve, plays the role of a thermal resistance through which the energy deposit inside the
 43 cell is evacuated towards the base.

44 The thermal flow difference between the two cells, proportional to the heating rate, is calculated thanks to
 45 temperature measurements and a calibration curve. This curve is done prior to any incore measurement, using a
 46 heater element located inside each cell and allows simulating the energy deposit by joule effect.

47 Note that the heating rate is written W/g (C) to emphasise the fact that it is relative to graphite. Devices for
 48 OSIRIS in-core measurements consisted of five different probes (each one made of four cells side by side, see
 49 cross section in Fig.1), piled-up along the core height leading to five measurement points, from which the heating
 50 profile curve was fitted. Inherent drawbacks of these calorimeters came essentially from the static nature of the
 51 technology. The heating distribution was plotted from only few measurement points, and the obtained distribution
 52 was restricted to the core height. In addition, each measurement point corresponded to a given calorimeter with
 53 its own calibration curve.

54 Furthermore, an accurate dimensioning of an experimental device requires as input data, the knowledge of the
55 axial distribution of heating but not restricted to the core itself. In addition, one of the major problems of this
56 static conception came from ageing effects under the radiation field, which can lead to difficulties for detecting
57 the decrease of the calorimeter sensitivity under irradiation.

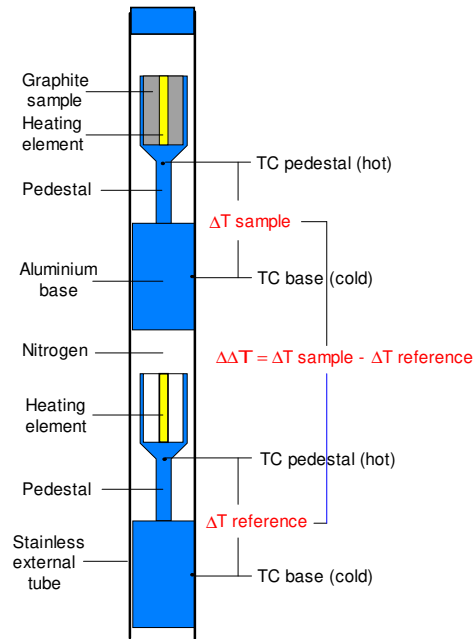
58 **2. New concept of the nuclear heating measurement**

59 To overcome inherent drawbacks of the previous technology, an innovative system has been studied, tested and
60 run in the OSIRIS reactor. The key point of this new sensor is setting two cells (one empty and one equipped with
61 the sample in which we evaluate the energy deposit), piled-up inside a same external sleeve, and then moving the
62 whole in the core with the help of a displacement system [8]. Therefore, advantages of such a new probe,
63 compared to the static one, are:

- 64 - To get a continuous heating profile instead of one deduced from only some points,
- 65 - To extend the axial measurement range above the core, where heating rates still remain high enough to be
66 taken into account,
- 67 - To suppress entirely the ageing effect, because of a probe being in the radiation field only during
68 measurement periods,
- 69 - To get all measurements by the same calorimeter, leading to a global consistency in the profile in terms of
70 relatives values,
- 71 - To have a complete coaxial sensor design, allowing to avoid any asymmetric effect, facilitating any further
72 modelling, therefore the comparison with calculation,
- 73 - To obtain pointwise measurements and to minimize any gradient effect thanks to a smaller size.

74
75 The new design is displayed in Fig 2. The upper cell contains a graphite sample, whereas the lower one is empty
76 (reference cell). A gas gap (nitrogen) surrounds each cell. They are set on a base inserted inside a stainless external
77 steel in contact with the water flow. A thermocouple (K type) is embedded on the top of each pedestal ("hot

78 temperature”) whereas a second one is located on the external surface of the base or at the bottom of the pedestal
 79 (“cold temperature”). Two heating elements composed by a constantan wire embedded inside an alumina pearl,
 80 located inside the cells, allow the calibration. The energy deposit in the massive part of the cells is flowing through
 81 the pedestal and then through the external sleeve.



82

83 Fig.2. CALMOS design with its two piled-up cells configuration.

84 The temperature difference “ ΔT_{sample} ” (see Fig.2) is proportional to the energy deposit both in graphite and the
 85 cell structure, whereas “ $\Delta T_{\text{reference}}$ ” is proportional to the only deposit in the empty cell structure. Therefore, in first
 86 approximation, if cells are identical, the difference “ $\Delta T_{\text{sample}} - \Delta T_{\text{reference}}$ ” quantity ($\Delta\Delta T$) is proportional to the
 87 energy deposit inside the only graphite sample. This new nuclear heating measurement method has been patented
 88 [7].

89 As both cells are superimposed in a same envelope (Fig. 2), measurements are performed in two steps at each
 90 altitude in the core, by moving the probe in the radiation field.

91 Along this R&D program, different phases followed each other, before reaching a complete device, which
92 allows incore measurements up to the nominal power:

- 93 - Two mock-ups have been successively manufactured and tested in the reactor periphery, up to a 2 W/g (C)
94 limited heating rate, to check the probe manufacturing and the measurement protocol,
- 95 - A first complete equipment CALMOS-1 (probe associated to a displacement system) has been tested
96 inside the core in the 2011-2013 period (during 8 cycles) [9, 16, 23] which allowed to have a significant
97 feedback, to highlight the required improvements on this first prototype so as to reach a real operational
98 measuring system,
- 99 - Finally, the CALMOS-2 device [28], has been manufactured, calibrated and tested during the last 3 cycles
100 in 2015. It is the updated version which can be considered as a qualified measurement device for incore
101 measurements. The automatic cell mobility, with a specific software through a Human Machine Interface
102 (HMI) allowed highlighting the different possibilities of this new sensor.

103
104 This paper relates the entire R&D program, from the conception, the modelling, the manufacturing, the
105 calibration and the qualification phase inside the core. Thanks to all results collected during the measurement
106 campaigns, a comprehensive analysis is presented.

107 However, for detailing the cell configuration, the last upgraded CALMOS-2 version is taken as reference.

108

109 **3. Calibration of the calorimeter**

110 Prior to any measurement, a calibration is performed in out of pile conditions [9]. Firstly, the calorimeter behavior
111 is checked in natural convection, directly into the pool of the reactor. A first calibration curve is done, and the linearity
112 is verified.

113 Secondly, we check that the calibration coefficient remains unchanged when the probe, set on its displacement
114 device, is placed on a bench simulating real thermohydraulic conditions. The slope of each cell ($^{\circ}\text{C}/\text{W}$) is measured.

115 The calibration procedure requires applying different electric powers to heaters (the constantan wire used for heaters
 116 limits the applied power to around 5W), and to measure pedestal and base temperatures after stabilization. If we
 117 consider that the heat transfer is only made by conduction through the pedestal, and applying the conduction law to
 118 calculate ΔT between hot and cold thermocouples (see Fig 2), a K calibration coefficient for the calorimeter is defined
 119 ($\text{W}\cdot\text{g}^{-1}\cdot\text{C}^{-1}$) by:

120

$$121 \quad K = \frac{1}{M_E P_E + m_V \cdot (P_E - P_V)} \quad (1)$$

122

123 Where P_E and P_V are the slopes ($^{\circ}\text{C}/\text{W}$) of sample and reference cells, M_E the graphite sample mass and m_V the total
 124 mass of structure (aluminum + heater) above the hot point (“hot temperature”). The term $m_V (P_E - P_V)$ relates to the
 125 difference of thermal responses between cells, due to inevitable slight manufacturing differences, and secondly to take
 126 into account that bases of the two cells are not exactly in the same environment. If sample and reference cells are in a
 127 same radiation field, the total heating rate E_T is given by:

128

$$129 \quad E_T = K_C(E_T) \cdot K \cdot \Delta\Delta T \quad (2)$$

130

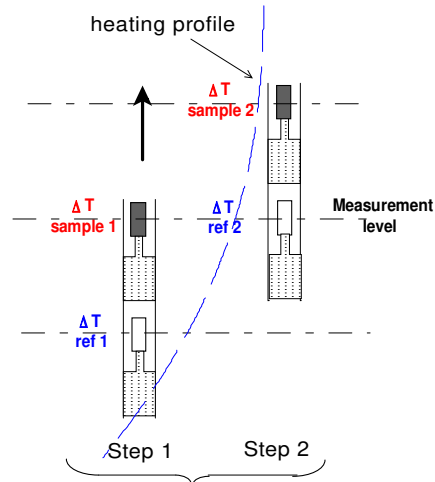
131 where $\Delta\Delta T$ is defined as $\Delta\Delta T = \Delta T_{\text{sample}} - \Delta T_{\text{reference}}$ and $K_C(E_T)$ to the nonlinearity coefficient. This latter
 132 depends of heat leakages by radiation or conduction in the gas and, on the other hand, on the conductivity dependence
 133 of aluminum with temperature. Lower are temperatures reached in the cell, better is the linearity [11]. $K_C(T)$ has been
 134 evaluated both by using the finite element model and thanks to measurements up to $13 \text{ W}\cdot\text{g}^{-1}$.

135 **4. Possible measurement ways with the new sensor**

136 *4.1 Use of the K coefficient from calibration*

137

138 Once the probe calibrated, the measurement in the radiation field is performed in two steps.



139

140

141 Fig.3. Procedure for the nuclear heating measurement in the radiation field of the reactor core.

142

143 Starting from a given static position in the radiation field, temperatures of the sample cell are recorded. Then,
 144 taking advantage of the moving system, the whole calorimeter is shifted (moved up or down), in such way that the
 145 reference cell position matches with the previous sample cell location. Temperatures of the reference cell
 146 are recorded. Then, heating is deduced using (2) when cells are at the same level. As shown in Fig.3 the displacement
 147 step by step allows drawing the entire heating profile. Note that the elevation step can be a subdivision of the distance
 148 between cells to draw the heating profile as finely as required.

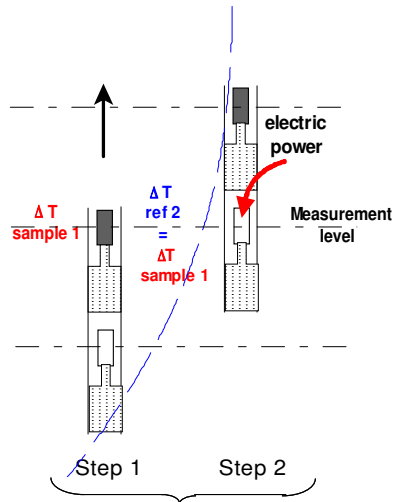
149

150 4.2 Use of the “zero method”

151

152 In addition to use the calibration phase, advantage of such a calorimetric sensor is offering another nuclear
 153 heating measurement so called the “zero method”. Fig.4 illustrates the measurement of heating through the “zero
 154 method”. The two cells being at the same altitude in the core, the nuclear energy deposit inside the sample can be

155 evaluated by adjusting an electrical power in the reference cell heater (simulating the energy deposit in the sample by
 156 radiation) so as to equalize ΔT sample and ΔT reference.



157
 158
 159 Fig. 4. The two cells being located at the same core level, the current intensity is adjusted inside the reference cell heater until to cancel the quantity
 160 “ $\Delta T_{\text{Reference}} - \Delta T_{\text{Sample}}$ ”.

161
 162 Then, the heating rate E_T in the sample is deduced from:

163
 164
$$E_T = \frac{W_e}{M_E} \cdot K_0 \quad (3)$$

165
 166 Where W_e is the dissipated electric power (W) in the reference cell and M_E the graphite sample mass (g). We note
 167 that K_0 is equal to 1 if both slopes are identical. As there are inherent small differences of thermal transfer capabilities
 168 (slopes in $^{\circ}\text{C}\cdot\text{W}^{-1}$) between the two cells, a K_0 correction factor is needed (the temperatures equilibrium is made with
 169 the reference cell):

170

$$K_0 = \frac{\frac{P_V}{P_E}}{1 - \frac{m_V}{M_E} \cdot \left(\frac{P_V}{P_E} - 1\right)} \quad (4)$$

171
172
173 With P_V an P_E the slopes in °C/W for the reference and the sample cells respectively, m_V the mass of the cell
174 corresponding to the part located the “hot” thermocouple and M_E the sample mass.

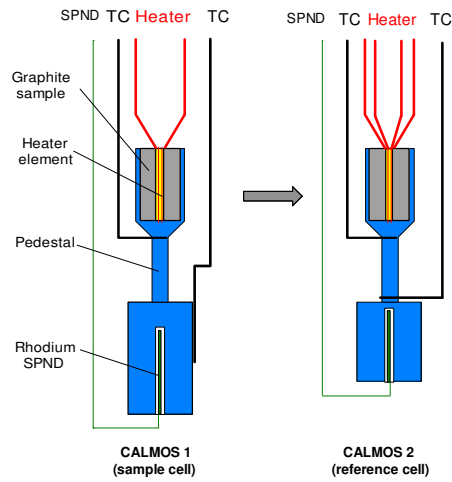
175 The “zero method” is considered as the most reliable measurement because it is performed without using the
176 preliminary calibration. To improve the reliability of this method, two major improvements have been implemented in
177 the last upgraded CALMOS-2 version [28] (Fig.5).

178
179 Position of thermocouples: Cells have not the same thermal transfer capability (slope in °C.W⁻¹), so the lower the
180 difference is, the lower the K_0 influence in equation (3) is. The best way to tend K_0 to unity is to limit the thermal
181 resistance between the two measurement points to the only Aluminum cylinder (pedestal, see Figs.5 and 6). The effect
182 is significant. The slopes discrepancy in the last version has been reduced to 0.3 % [28]. The K_0 correction coefficient
183 is now close to 0.99 (0.955 for CALMOS-1). By that way, performing a measurement using the zero method is nearly
184 independent of slopes measurement, i.e of the calibration phase.

185 Power measurement: In addition to considering that the heat dissipation inside the heater element is fully
186 representative of the energy deposit by nuclear heating, we need also to be confident on the power measurement
187 during the equilibrium phase.

188 Calculations of the We energy deposit assume that the effective resistance r of the heater element is well known,
189 and more importantly, that r does not change with ageing, temperature or irradiation conditions. Therefore, to measure
190 more accurately the energy deposit by joule effect, and to avoid any assumption about the resistance evolution in the
191 reference cell, this latter is equipped with a 4-wire element heater element, two wires for the intensity and two for the
192 voltage measurement (Figs. 5, 6).

193



194

195

196 Fig.5. Evolution of thermocouples locations and heater wiring to improve the “zero method” accuracy.

197

198 Therefore, the applied electric power to the heater is measured by $W_e = U I$ (U the voltage, I the intensity) instead of

199 $W_e = r I^2$. Such implementation led to one of the major difficulty in the manufacturing, because the whole wiring has

200 to be inserted inside an overall 17mm diameter, each wire insulated from each other.

201



202

203

204 Fig.6. CALMOS-2 details: upgraded position of thermocouples located at the top and bottom of the pedestal (left), and implementation of a 4-

205 wire resistance inside the reference cell of the calorimeter (right).

206 5. Numerical modeling of the sensor

207 5.1 Modelling of the sensor

208

209 Temperatures inside the probe were required prior experiments for safety reasons. These temperatures were
210 calculated using a Finite Element model of the sensor. This model was built using the FE CAST3M calculation
211 code [24]. The whole probe was modeled using an axisymmetric description. Only very few simplifications were
212 made on the cell description. Main ones are the suppression of the wires connecting the cells to the outside and
213 the suppression of the rhodium SPND inside the lower base. The upper part of the device (sealed passage and
214 above) was somewhat simplified since it plays only a secondary role on the measurement process. Fig. 7
215 displays the sensor meshing, to be compared with Fig. 9.

216 For practical reason, a small gap had to exist between each cell base and the external sleeve. It allows
217 inserting the cells inside the sleeve during the sensor manufacturing. This mechanical clearance was determined
218 from dimensional measurements. It is very small (24 micrometers at ambient temperature) but had to be
219 considered in the FE model to get accurate results.

220

221

222

223

224

225

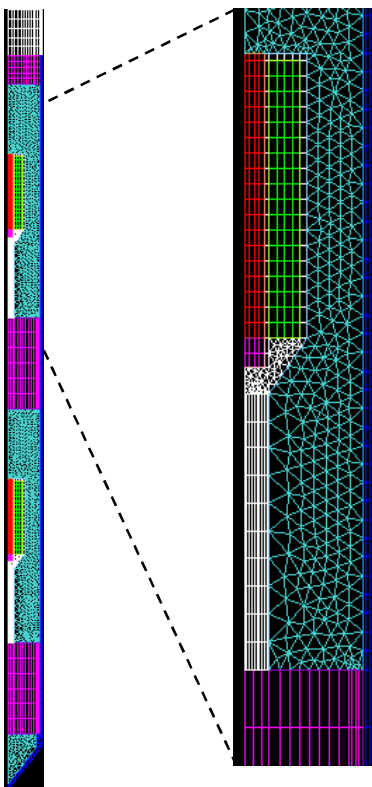
226

227

228

229

230



231
232
233
234
235
236
237
238
239
240
241
242
243
244
245

246 Fig.7. Meshing of the whole calorimeter (left) with focus on the sample cell (right)

247

248 Indeed, this gap is filled with nitrogen, which has a very low thermal conductivity ($0.026 \text{ W}\cdot\text{m}^{-1}\text{K}^{-1}$ at 27°C). It
249 insulates the cells from the outside and has an important effect on absolute temperatures inside the cells. In the
250 FE model, the gap width was set to depend on temperatures since thermal dilation coefficients of aluminum ($25 \times$
251 10^{-6} K^{-1} at 25°C) and stainless steel ($16.5 \times 10^{-6} \text{ K}^{-1}$ at 25°C) are different. In order to avoid micrometer size
252 meshes (gap between the external surface of aluminum bases and the internal surface of the steel sleeve) aside to
253 millimeter ones (steel sleeve), a local apparent conductivity of the stainless steel located in front of the gap is
254 calculated (postulating a two cylinder serial configuration) and used at different steps of the FE simulation.

255 Physical characteristics of the different materials play a key role on the obtained results. Values of heat
 256 capacity (C_p), thermal conductivity (λ), coefficient of expansion (α), volumetric mass (ρ) and their dependence
 257 with temperature have been taken in literature. As thermal characteristics of aluminum AW1050 have a
 258 significant impact on temperatures inside the cells, a specific determination by measurements was ordered to a
 259 metrology specialized laboratory [27]. Except for the volumetric mass which is considered constant at 2670 kg.m^{-3} ,
 260 other data were used in the last version of the FE model [25, 26]. They are summed up in Table 1.

261

T (°C)	ρ (kg.m^{-3})	C_p ($\text{J.K}^{-1}.\text{kg}^{-1}$)	λ ($\text{W.m}^{-1}\text{K}^{-1}$)
24	2684	886	
100	2668	939	24.8
200	2648	982	25.2
300	2627	1018	25.6
400	2605	1059	26.3
500	2582	1109	27.2

262

263 Table 1. Thermal characteristics of the aluminum AW1050.

264

265 In the FE calculation, the thermal power is injected in the device as a specific power (W.g^{-1}). The same
 266 specific power is used for all different components of the calorimetric cell regardless the atomic number of their
 267 constituting material. This assumption was considered as appropriate considering previous experiments made
 268 inside the OSIRIS reactor.

269 Velocity of water around the probe was measured on an experimental bench before putting the measurement
 270 device in real conditions in the reactor. This velocity value was used to calculate the Reynolds number and then
 271 the thermal flux exchanged between the probe and the pool using the Dittus Boelter correlation. Water

272 temperature inside the device (internal flow in the displacement system, see Fig. 18) was measured by dedicated
273 thermocouples.

274 On the other hand, a polished mirror is placed around the cell in the design. That allows to limit heat losses by
275 radiation by adjusting in the cell the internal walls emissivity. Nevertheless, this thermal screen is not perfect. A
276 sensitivity study performed on the CALMOS-1 cell (very similar to CALMOS-2), using an aluminum surface
277 emissivity of $\epsilon = 0.05 \text{ W.m}^{-1}\text{K}^{-1}$ and $\epsilon = 0.01 \text{ W.m}^{-1}\text{K}^{-1}$, led to a 1.4 % difference on the calculated heating rate E_r
278 (temperature of the graphite is roughly 500 °C). As it is very difficult to determine which coefficient to use, and
279 as the effect remains small, we chose not to take into account radiative thermal losses in the CALMOS-2 model.
280 Fig. 8 shows an example of temperature map obtained for in pile conditions when a 13 W.g^{-1} heating rate is
281 applied in the FE model.

282

283

284

285

286

287

288

289

290

291

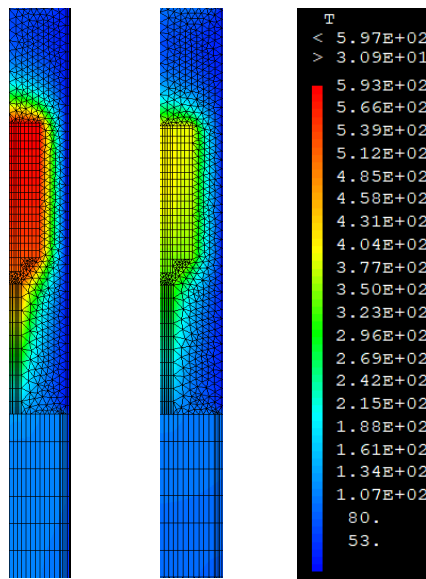
292

293

294

295

296



297

298

299

300

301

302 Fig. 8. Example of temperature distribution inside the cells obtained for 13 W/g with FE modelling (left: sample cell; middle: reference cell;
303 right: temperature scale).

304

305 *5.2 Comparison between calculations and measurements*

306

307 The first comparison is made on experimental results obtained during the calibration process of the probe. As
308 the simulation is concerned, the Joule electric power is injected as a volumetric power applied inside the alumina
309 pearl volume (element heater). Water temperature surrounding the probe is measured during the experiment.
310 Fig.13 shows that calculated results are in very good agreement with experimental data. However, the range of
311 power variation is limited because the total energy applied to the element heater (4.5 W in Fig.13) corresponds
312 roughly to a simulated 5 W.g⁻¹ heating rate.

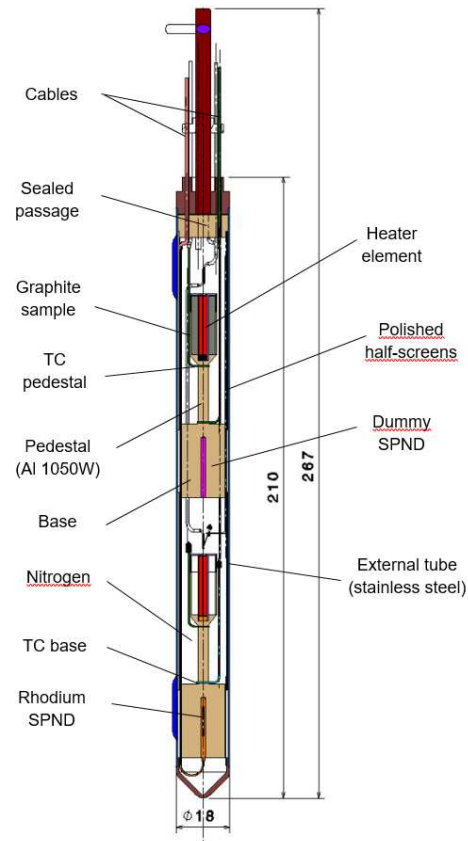
313 On the other hand, comparisons were made with measurements performed in real OSIRIS incore conditions.
314 Results agree quite well for low to medium nuclear powers. For highest values, some discrepancies appear
315 leading to a nonlinear behavior between the input nuclear power and the calculated one. One part of these
316 discrepancies could come from the behavior difference between both cells regarding the thermal radiative flux
317 (heat losses by radiation), despite the use of mirror-polished screens located around the cells. Another source of
318 nonlinearity could come from the non-symmetric axial environment of both cells. We tried in other papers to
319 calculate the $K_c(E_T)$ (2) factor in order to correct these non-linearity effects. Nevertheless, even if interesting
320 results are obtained, it is difficult to assert the value and could not confirm the non-linearity evolution, which has
321 been experimentally found and presented in Figs. 23 and 36.

322 6. Optimized characteristics

323 Fig.9 shows a cross section of the final CALMOS-2 calorimetric probe. Taking into account thermohydraulic
324 conditions, mechanical constraints, and incore conditions requirements, optimized values for main dimensions are
325 [28]:

- 326 - Base: AW1050 aluminum, 17 mm in diameter, 25 mm height,
- 327 - Pedestal: aluminum, 3.8 mm in diameter, 20 mm height, 20 mm between TCs locations,
- 328 - Sample: graphite
- 329 - Cell upper part: sample weight 1.432 g, 8 mm in diameter, 20 mm height,
- 330 - Mass of the cell upper part 1.621 g,
- 331 - External sleeve: stainless steel 0.5 mm thick, overall height 210 mm,
- 332 - Internal gas: N₂, capsule pressure 1.5 bar,
- 333 - Half-screens: stainless steel, 0.2 mm thick,
- 334 - Heater: constantan wire, 0.25 mm in diameter, resistance 1.8 Ω, 4-wire resistance for the reference cell, 2
335 A maximum,
- 336 - Distance between cells: 88 mm,
- 337 - SPND: Rhodium emitter 0.5 mm in diameter, 10 mm length.

338 The picture in Fig. 10 illustrates the preliminary assembly of both cells, before their insertion inside the
339 external sheath, with upper polished half-screens not assembled yet.



340

341 Fig.9. Overall cross section of final design of the calorimetric cell (CALMOS-2 configuration).

342



343

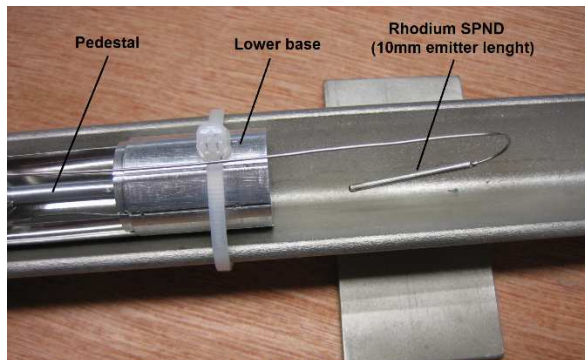
344

345 Fig.10. Intermediate step in the CALMOS-2 manufacturing. The two cells are in a temporary guide and thermocouples are put into place,
346 but polished half-screens are not assembled yet.

347 7. Measurement of the thermal neutron flux

348 Measurement of the conventional thermal neutron flux (flux normalized to the 2200 m/s neutron speed) is
349 made thanks to a Rhodium SPND, especially designed to fit the calorimeter cell geometry. This SPND is similar
350 in terms of material and cross section to the standard one used for many years in OSIRIS reactor, but with a
351 rhodium emitter length reduced to only 10 mm whereas the standard one is 50 mm. The total length is around 20
352 mm allowing its implementation inside the aluminum cell base. In CALMOS-1 the SPND is embedded inside the
353 upper cell (around mid-height of the sensor) whereas for the last version it is embedded inside the lower cell. This
354 change allows extending the accessible length by more than 100 mm in the core axis with CALMOS-2 (Fig. 21).
355 The lowest accessible altitude for the first version is -191 mm/core mid-place against -294 mm for the updated
356 one. This improvement is significant with regard to a total fissile height of 640 mm.

357



358

359

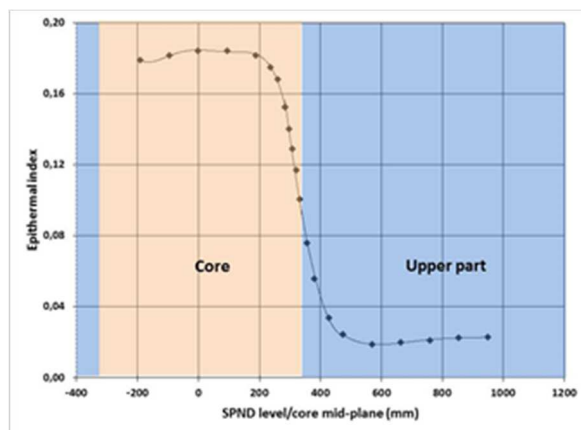
360 Fig.11. CALMOS-2: Shaping and introduction of the specific SPND (rhodium emitter 0.5mm in diameter, 10mm length) inside the lower
361 base (overall length 20mm).

362

363 The rhodium emitter offers a good sensitivity, but the capture reaction $^{103}\text{Rh}(n, \gamma)^{104\text{m}}\text{Rh}$ used for establishing
364 the signal (current intensity) has a response both in thermal and epithermal ranges. The thermal flux measurement
365 needs to be made along the entire mechanical stroke, from -160 mm to +960 mm/core mid-plane. However, the
366 neutron spectrum varies a lot along this range and needs to be calculated for deducing the thermal flux from the
367 delivered intensity.

368 The epithermal index (epithermal neutron flux/thermal neutron flux) characterizes the spectrum for energies in
369 the thermal range and is used to process the SPND signal. It is calculated inside the cell with the TRIPOLI-4®
370 Monte Carlo code at the precise location of the SPND and for any accessible altitude in the core [12, 21]. Fig 12
371 shows the evolution of this index calculated inside the 64 experimental location. Note that the index decreases
372 sharply at the fuel-moderator transition to become ten times lower in water. The relative contribution to the total
373 current of the SPND due to the epithermal contribution is around 5 % in the upper part of the core (in full
374 moderator) whereas it can reach around 48 % at the core mid-plane. This shows that the epithermal index
375 knowledge, all along the CALMOS mechanical stroke, is of major importance for using a Rhodium SPND
376 located inside the calorimetric cell.

377



378

379

380 Fig.12. Calculated epithermal index (epithermal neutron flux/thermal neutron flux) evolution in the 64 experimental location along the total
381 mechanical stroke of the calorimeter. The associated uncertainty is less than 1 %.

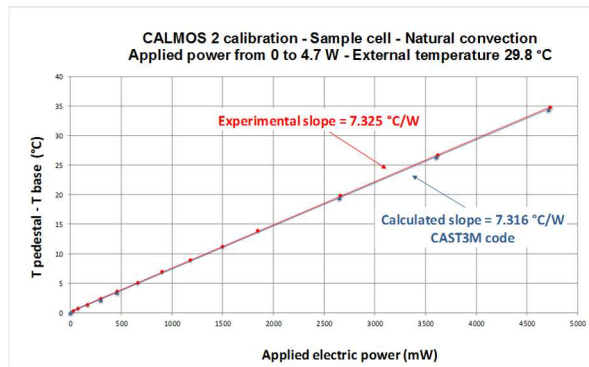
382 **8. Results of the calibration**

383 The calibration phase (see chapter 3) is performed in no radiation conditions and in both natural and forced
384 convection. The purpose is to determine not only the K calibration coefficient (1), linking the $\Delta\Delta T$ measurement
385 to the nuclear heating rate E_T , but also the time constant of the calorimeter, i.e the time necessary to get a
386 stabilized temperature map inside the calorimetric probe. During the calibration following key points are
387 measured:

- 388 - The cell slopes ($^{\circ}\text{C}/\text{W}$) from which K is deduced and the slopes linearity up to a 5 W electric power,
- 389 - The independence of both cells. The electrical power is applied in heaters separately or simultaneously to
390 both reference and sample cells. It is essential to check that there is no influence of cells on each other,
- 391 - The validation of the K coefficient in forced convection conditions,
- 392 - The time constant of the calorimeter, defined in this experiment as the time required to reach 99 % of the
393 stabilized signal after a transient. That drives the total time required to draw heating profiles in the reactor.

394
395 Fig. 13 shows the result of the slope measurement of the CALMOS-2 sample cell, illustrating the excellent
396 linearity up to a 4.7 W applied to the heater element. In the same figure is plotted also the determination by
397 calculation performed with the CAST3M finite element model (see chapter 5). The C/M ratio is less than 0.15 %.
398 However, for this low level of power, the whole energy deposit in the upper part of the cell is entirely evacuated
399 by conduction through the pedestal. We do not have any heat leakage (radiation, conduction in gas) to take into
400 account in the modelling.

401



402

403

404 Fig.13. Experimental determination of the sample cell slope of the CALMOS-2 probe in natural convection.

405

406 Table 1 gathers all results of slopes determination and permits to illustrate that:

- 407 - The slope of the sample cell is very close to the reference one. That demonstrates the manufacturing
- 408 accuracy and also, the weak influence of unavoidable discrepancies in the thermocouples setting along
- 409 each pedestal,
- 410 - The two different thermohydraulic conditions lead to a maximum of 1.8 % dispersion on the slope
- 411 determination (case of reference cell, separated heating). Such a discrepancy is included in measurement
- 412 uncertainties,
- 413 - The heating mode (separated or simultaneous) has no influence on slopes determination, demonstrating
- 414 that there is no significant thermal influence between both cells. It is a critical point to validate the “zero
- 415 method” protocol, at least up to a 5 W applied electric power,
- 416 - Among all configurations, the dispersion is less than 1.3 % for the sample cell against 1.9% for the
- 417 reference one.

418

419 To check results obtained in natural convection, tests performed on the hydraulic bench were limited to only 2

420 applied electric powers covering the whole 5 W energy range. Therefore, the final K calibration coefficient,

421 retained for the CALMOS-2 exploitation, is the average of the two results obtained in separated and simultaneous
 422 heating, and in natural convection.
 423

Thermo hydraulic conditions	Natural convection ($\approx 30\text{ }^{\circ}\text{C}$)		Forced convection ($\approx 40\text{ }^{\circ}\text{C} - 1.24\text{ m}^3\cdot\text{s}^{-1}$)	
	Sep.	Sim.	Sep.	Sim.
Heating mode				
P _s slope ($^{\circ}\text{C}\cdot\text{W}^{-1}$)	7.325	7.337	7.418	7.388
P _R slope ($^{\circ}\text{C}\cdot\text{W}^{-1}$)	7.301	7.294	7.432	7.344
K ($\text{W}\cdot\text{g}^{-1}\cdot^{\circ}\text{C}^{-1}$)	0.0950	0.0945	0.0943	0.0939
K Retained value ($\text{W}\cdot\text{g}^{-1}\cdot^{\circ}\text{C}^{-1}$)	0.0948			

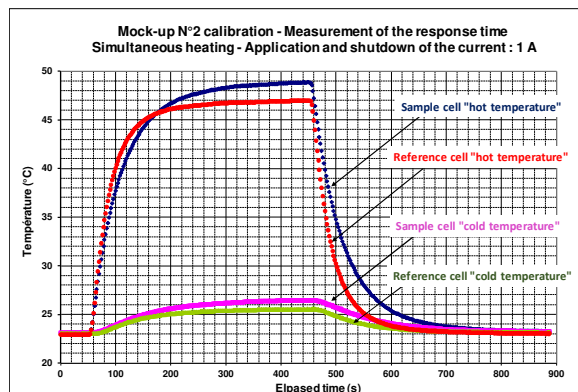
424

425 Table 2. Experimental results of CALMOS-2 calibration.

426

427 The second major parameter is the calorimeter response time (or time constant), which is an important
 428 criterion. It must be taken into account to define, before starting measurements, the allowed definition (number of
 429 steps) compatible to the possible modification of the radiation field (control rods movement) during the expected
 430 duration of the total scanning. As this time depends on cooling conditions, it is measured in natural and forced
 431 convection [13, 19]. Preliminary tests, performed on the two mock-ups (illustrated in Fig. 14), showed that the
 432 response time measured during a temperature rise is slightly higher to the time measured during a decrease
 433 (roughly 15 s over a 250 s total time). On the other hand, in natural convection, the presence of the external

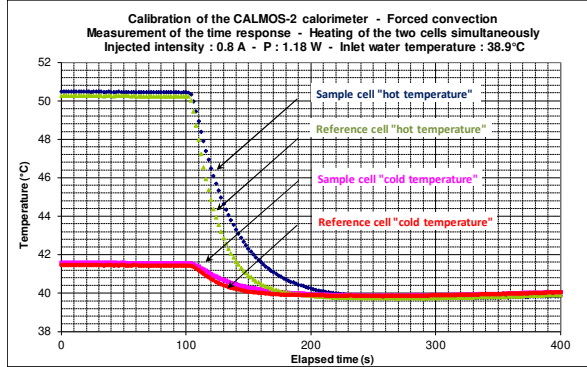
434 sheath (required for a calorimeter in incore conditions) leads to increase the response time (roughly 8 s over a 250
 435 s total time). Indeed, when the calorimeter is inside its external sheath (situation illustrated in Fig.18), the heat
 436 extraction is ensured by the only 1.5 mm static water gap surrounding the calorimeter (in natural convection).
 437 Such situation occurs when primary pumps stop (no primary flow).
 438



439
 440
 441 Fig.14. Measurement of the response time on the mock-up N°2. Evolution of temperatures during a power transient, after application and
 442 shutdown of a 1 A intensity in both element heaters.

443
 444 Therefore, the measurement of the time constant of calorimetric cells, when set on their displacement systems
 445 (CALMOS-1 and 2), are performed by recording the temperature decrease, first to measure the longest time
 446 constant of the whole cell, and secondly to avoid any constraint involved by applying a too much sharp step of
 447 power to element heaters. To perform this measurement, a 0.8 A is applied to both heaters until thermal
 448 equilibrium. After turning off the current, temperatures are recorded (example in Fig. 15). The analysis of Figs.
 449 14 and 15 shows that the time response of the sample cell is longer than the reference one, due to the additional
 450 thermal inertia induced by the graphite. Table 2 refers to results obtained in natural and forced convection for the
 451 CALMOS-1 calorimeter, similar to the last version. It gathers measured values corresponding to times required to
 452 reach 99 % of the stabilized signal. Obviously, it shows a significant gain of time response when using the
 453 OSIRIS forced convection.

454



455

456

457 Fig.15. Measurement of the CALMOS-2 calorimeter response time by a decreasing transient.

458

459 For the OSIRIS thermohydraulic conditions, the response time of the sample cell is close to 2 min 30 s. That
 460 value governs the total time required to reach the temperatures stabilization in the whole probe, after any change
 461 of position in the reactor radiation field. Table 2 shows also that, when the sensor is used inside the core but
 462 without primary flow (measurement at very low reactor power or follow-up of the residual power) the waiting
 463 time to make a heating measurement requires a total time at least 30 % longer.

464

Conditions	Natural convection	Forced convection	Discrepancy (N-F/N)
Sample cell	210 s	155 s	-26%
Reference cell	150 s	90 s	-40%

465

466 Table 3. Experimental results of the response time measurement on the CALMOS-1 calorimeter.

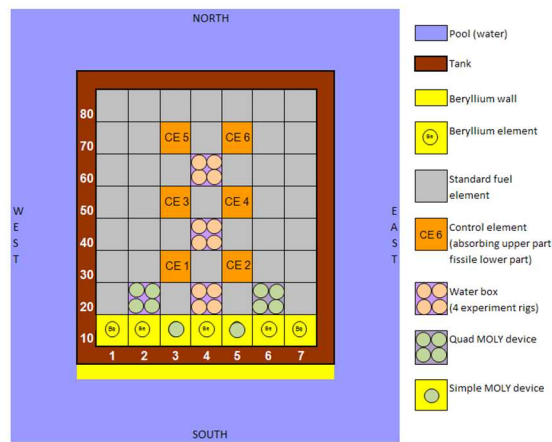
467

468 Note also that using the AW1050 Aluminum alloy for the cells allowed reducing the response time due to its
 469 higher thermal conductivity. ($230 \text{ W}\cdot\text{m}^{-1}\cdot\text{K}^{-1}$ against $130 \text{ W}\cdot\text{m}^{-1}\cdot\text{K}^{-1}$ for the AW 5754 alloy at around $100 \text{ }^\circ\text{C}$)[26,
 470 27].

471 9. Generalities about the OSIRIS reactor

472 OSIRIS was a pool type light water reactor with an open core. The core itself is a compact unit, with an
 473 horizontal section of $60 \text{ cm} \times 70 \text{ cm}$ and a height of 70 cm . The core housing contains a rack of 56 cells. This
 474 rack is loaded with 38 standard fuel elements, 6 control elements and up to 7 beryllium elements. At least two
 475 experimental locations (22 and 26) are dedicated to radioisotopes production for medical application (MOLY
 476 devices). Remaining locations (24, 44 and 64) receive experiments, and are equipped with water boxes ($82 \text{ mm} \times$
 477 82 mm) which can contain up to 4 experiment rigs (37 mm in diameter) (see Fig. 16).

478



479

480 Fig.16. Horizontal cross-section of the OSIRIS core

481

482 Purpose of the CALMOS device is making measurements in 24, 44 and 64 locations. The core configuration
 483 is such that the heating level is higher when we go from the south to the north, i.e 24 then 44 and finally 64. All
 484 measurements carried out from 2013 to 2015 with CALMOS-1 and CALMOS-2, and detailed hereafter, were

485 carried out in various core conditions (start-up, steady state, shutdown, core loading, rods positions and
486 configuration of experimental devices).

487 **10. Description of the displacement system**

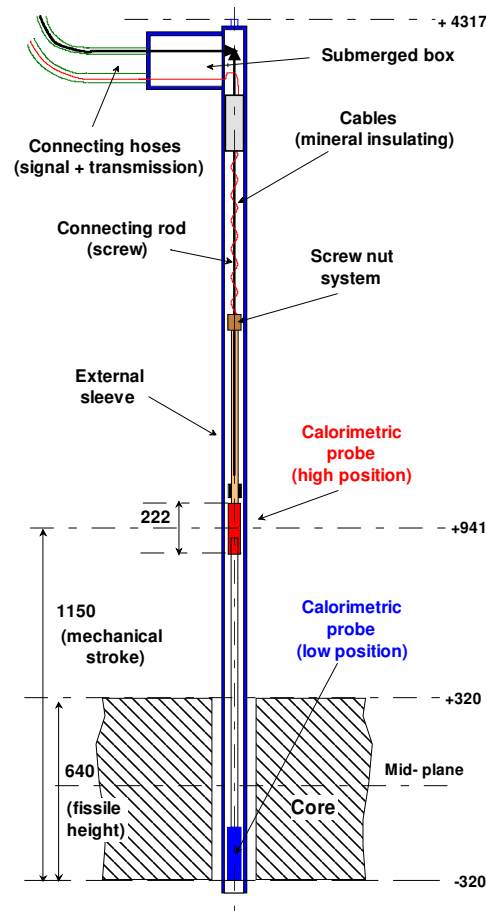
488 The study of the displacement system, allowing the movement of the calorimetric cell inside the core is as
489 important as the development of the calorimetric cell itself. This device needs to answer not only to conditions for
490 performing a measurement inside the core, but also as a standard incore experiment, to meet all conditions in
491 terms of reactor safety.

492 Main purpose of this paper is not detailing this part of the R&D program. However, a short description is
493 given hereafter to illustrate the working mode, objectives, limits, and difficulties for moving a probe inside an
494 experimental reactor. The challenge to cope with was to get incore axial distributions while preserving
495 permanently both same measurement conditions and the required safety margins.

496 The complete device is in two parts: the calorimetric cell and the displacement system. The device is set inside
497 the core before reactor start-up, and taken out after the end of the cycle. It is inserted into a water box (reactor
498 equipment) and inside one of the four available experimental locations (Fig. 17).

499 The displacement system is mainly made of an external sleeve (composed of aluminum and stainless steel)
500 inside which the calorimetric probe moves along a 1150 mm mechanical stroke corresponding to the core fissile
501 height and 510 mm above fuel elements, as shown in Fig. 17. Inside the connection box (link between out of pile
502 and in pile cables), placed above the pool surface 7 m away from the upper part of the displacement system (not
503 visible on Fig. 17), an electric engine rotates a cable inside its own sheath (mechanical transmission). This
504 rotation movement is transferred from the connection box to the submerged box. Inside this latter, located at the
505 top of the displacement system (around 4 m above the core mid-plane), a mechanical connection is made thanks
506 to a gearing set between the cable and a connecting rod, itself linked to the mobile equipment. From the bottom to
507 the top, the mobile equipment of CALMOS is made of the probe itself linked to the insertion tubes, themselves
508 connected to a screw nut system, itself connected to the connecting rod. By rotation on its axis, the cable moves

509 the whole vertically inside the external sheath. Two flexible hoses connect the submerged box to the upper
 510 connection box (Fig. 8), the first being dedicated to the mechanical transmission (cable in rotation) and the
 511 second one to the cell signals (thermocouples and rhodium SPND).
 512



513
 514 Fig.17. Main components of the displacement system equipped with the calorimetric probe (in blue and red according to the position).
 515

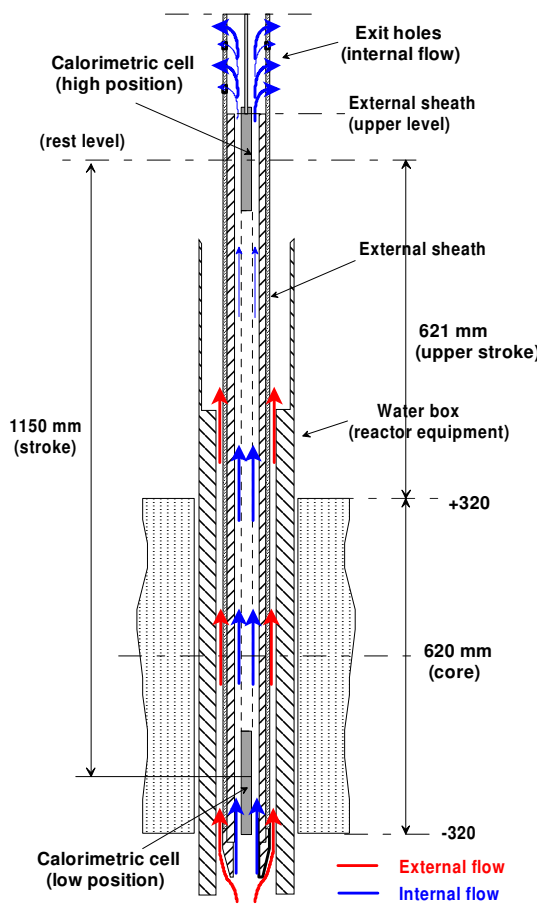
516 Main requirements for the displacement system are:
 517

- 518 - Ensuring a relevant heating measurement, as close as possible to the actual heating inside a standard
519 experiment used for material irradiation. The material composition on the 37 mm cross section (water +
520 external sleeve + calorimeter) must be as close as possible to the standard experimental capsule,
- 521 - Ensuring a displacement range as large as possible; the total mechanical stroke is 1150 mm
522 corresponding to the fissile height of fuel elements and a sufficient height above,
- 523 - Offering a rest position for the calorimeter. The highest altitude of the cell is around 900 mm with regard
524 to the core mid-plane (see Fig. 17). At this position, the estimated residual heating rate is less than 30
525 mW.g⁻¹ and the thermal neutron flux level less than 10¹¹ n.cm⁻².s⁻¹, avoiding any significant ageing effect
526 on the probe,
- 527 - Centring the calorimetric cell (18 mm in diameter) along the vertical axis which has a 37 mm internal
528 diameter,
- 529 - Ensuring the role of guide and housing for all the cables required for measuring the signals. That was the
530 major difficulty in the design. The cables, with mineral insulation and stainless steel sheath (1mm in
531 diameter), are twisted together in a spring shape so as to accommodate the 1150 mm total stroke by
532 successive stretching and compression,
- 533 - Ensuring appropriate cooling conditions of the probe whatever its altitude in the core. If ΔT sample and
534 ΔT reference temperature differences do not depend on the water cooling temperature and the water flow
535 (but only to the heating rate), absolute temperatures reached inside the cells depend directly on cooling
536 conditions. The hottest allowed temperature inside the cell structure is fixed to 500 °C in order to keep a
537 sufficient margin against aluminum melting [26]. Therefore, it is essential to ensure a good cooling. The
538 design allows to cool both the external sheath (external flow) and the mobile equipment (internal flow).
539 This internal cooling flow enters the sheath tube through its base (located under the fissile height of the
540 core) and exits through several holes located above the probe rest position (Fig. 15). In nominal
541 conditions, the internal flow is 1.35 m³.h⁻¹ (measured on a specific hydraulic bench representative of
542 OSIRIS conditions) corresponding to a 3.2 m.s⁻¹ linear speed around the probe. The cooling flow

543 variation does not exceed 12 % for a probe running from the top to the bottom of the total mechanical
 544 stroke.

545 In addition, the system has to meet the safety requirements in terms of reactivity. The insertion of the
 546 mobile equipment in the sleeve changes the local composition of the water box as the descent
 547 progresses, involving a reactivity effect on the core.

548



549

550

551

552 Fig.18. Cooling water flows inside the CALMOS device, when located inside an experimental location of the OSIRIS core.

553

554 Therefore, this effect has to be evaluated to check that, first, it does not disturb reactor operation in terms of
555 safety and, secondly, that the control rods movement for compensating this effect does not modify the radiation
556 field we are measuring. Results of this study are:

- 557 - Calculation showed that, whatever the experimental location, the reactivity effect induced by the total
558 insertion of the mobile equipment does not exceed 70 pcm. Such low impact complies with OSIRIS
559 safety requirements,
- 560 - To avoid any disturbance on the reactor, the vertical speed of the probe during the insertion phase is
561 limited to 5 mm.s^{-1} , leading to a reactivity effect less than 0.5 pcm.s^{-1} . In practice, to add a margin, the
562 vertical speed was further limited to 1 mm.s^{-1} when the cell goes through the fissile height of the core.
563 As a result, no disturbance on the reactor operation was noticed during measurement campaigns,
- 564 - The double monitoring of the radiation field by two devices located side-by-side in the same 64 location
565 (detailed in § 18), showed that the disturbance led by one calorimeter progression inside its own sheath,
566 does not involve significant changes in the close vicinity i.e in adjacent locations in the same water box.

567 **11. Generalities about incore measurement campaigns**

568 For each CALMOS device, a comprehensive measurement campaign has been carried out inside the core. The
569 CALMOS-1 measurement campaign lasted 10 OSIRIS cycles, corresponding to 8 cycles for the prototype itself
570 and 2 additional ones for the comparison with the updated CALMOS-2 version. Taking into account the
571 scheduled final shutdown of the reactor, planned at the end of 2015, the development, manufacturing, calibration
572 and all the tests of this last configuration had to be done during the only last 3 cycles of OSIRIS reactor. To
573 qualify CALMOS devices, the following kind of tests were carried out:

- 574 - Three incore locations, 24, 44 and 64 (in ascending order of heating rate), were measured. We remind
575 that a single location can be investigated per cycle,
- 576 - For the only device CALMOS-2, 21 complete automatic scanning were performed,
- 577 - Follow-up of the reactor start-up with the probe located at the core mid-plane,

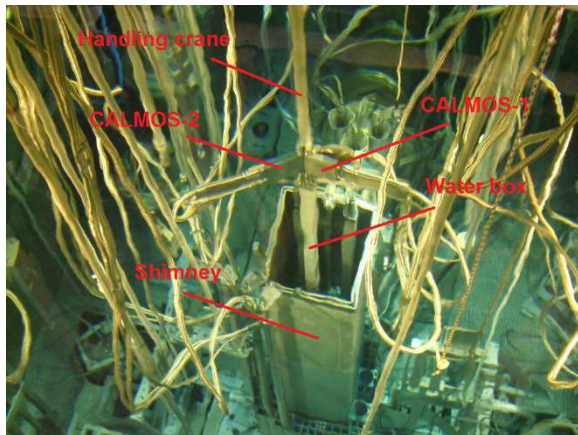
- 578 - Follow-up of the residual power decay with the probe located at the core mid-plane,
- 579 - Measurement of the mutual influence, in terms of heating and thermal flux, between both devices when
- 580 they are placed side-by-side in a same location,
- 581 - Comparison of CALMOS and MEREVER devices in terms of thermal neutron flux,
- 582 - Measurement of the reactivity effect consequently to the insertion of the mobile equipment inside the
- 583 core,
- 584 - Influence of the probe displacement speed on the core reactivity,
- 585 - Performing various measurements with the zero method, covering the 0-4 W.g⁻¹ heating range,
- 586 - Measurement of separated distributions (nuclear heating or thermal neutron flux),
- 587 - Measurement of simultaneous distributions (nuclear heating and thermal neutron flux),
- 588 - Test of all possibilities offered by the HMI system to set the parameters before the scanning (scan step
- 589 from 88 to 11mm, moving-up or moving-down, waiting time at each step, data acquisition for a long
- 590 time...).

591

592 All these tests required, for the only CALMOS-2 device, the total following durations:

- 593 - 3 monitored cycles (F282, F283 and F284),
- 594 - A total 14 hours recording time of the start-up phase, from 0 to the nominal power,
- 595 - A 74 hours total duration of automatic scanning time, thanks to the specific software and the human
- 596 machine interface (HMI),
- 597 - More than 19 days monitoring time of the residual power decay.

598



599

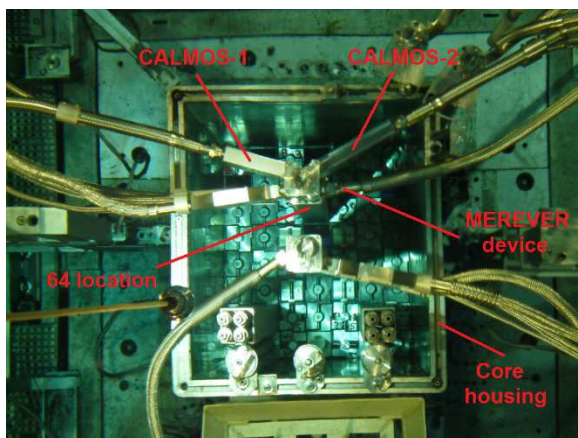
600

601 Fig. 19. Moving down of the loaded water box, equipped with both CALMOS devices, with the handling crane inside the 64 experimental
602 location.

603

604 Fig 19 shows the F284 loading phase (with CALMOS devices in the same water box which is being put into
605 place but not completely inserted yet), while Fig.20 shows a top view of the final configuration after the loading
606 completion, just before reactor start-up.

607



608

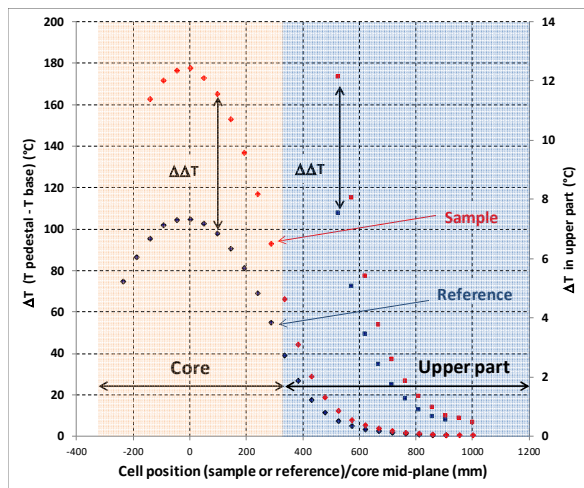
609

610 Fig. 20. Loading configuration of the core during the last F284 OSIRIS cycle. Both CALMOS prototypes are located side-by-side in the
 611 incore 64 experimental location (respectively 64NW and 64 NE positions). In addition, the MEREVER device dedicated to thermal flux
 612 measurement is in the same location in 64South-East position.

613 12. Establishment of the nuclear heating profile inside the core

614 To illustrate the way of performing the heating profile in the core, Fig. 21 shows an example of signal
 615 acquisition in the 24North-East location. On the same graph are plotted at each scan step (here 48 mm) ΔT
 616 sample, ΔT reference and their difference $\Delta\Delta T$, from which the nuclear heating is calculated (2). In case of
 617 CALMOS-1, the lowest position (under -139 mm) is not accessible with the sample cell, whereas above the core
 618 the highest position (above +906 mm) is not accessible with the reference cell, due to the probe configuration
 619 made up of a cell superimposed to another one with a 95 mm separation distance (88mm for CALMOS-2).
 620 Magnification scale (on right) permits to observe variations above the core.

621 In Fig. 22 are plotted together normalized values (to unity) of ΔT sample, ΔT reference and $\Delta\Delta T$ the difference
 622 among them. If the only quantity representative of the energy deposit in the sample graphite is $\Delta\Delta T$, the relative
 623 distribution can be obtained by each ΔT measurement (sample, reference or their difference).



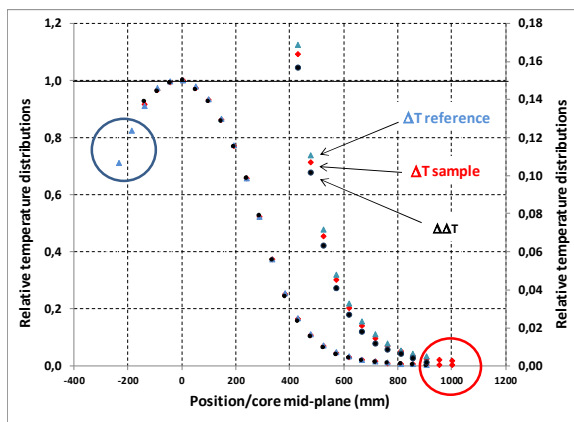
624

625

626 Fig. 21. Example of signals acquisition in 24North-East location of the core. Temperatures of ΔT sample and ΔT reference are recorded along
 627 the 1150mm total stroke. The core fissile height is between +/- 320 mm vs the core mid-plane (zoom in right scale).

628
 629 The three distributions are very close to each other. That is an important remark. That allows deducing the
 630 absolute distribution of heating in the reactor with only one measurement at a given altitude and with one of the
 631 three possible relative distributions.

632



633

634

635 Fig. 22. Distributions normalized to unity of ΔT sample, ΔT reference and $\Delta\Delta T$ in the 24North-East location of the core obtained by
 636 CALMOS-1 (zoom in right scale).

637

638

639 On the other hand, that allows extending the heating profile on highest and on lowest altitudes (blue and red
 640 circles in Fig. 21), for which it is impossible to measure the $\Delta\Delta T$ quantity due to the two superimposed cells
 641 configuration (Fig. 2). The highest altitudes are inaccessible to the empty cell, whereas lowest altitudes are
 642 inaccessible to the sample one.

643 **13. Test of the zero method and evaluation of the nonlinearity**

644 The “zero method” is the research of the equilibrium between cells, by balancing the nuclear energy deposit in
 645 the sample by a joule effect in the reference one. This method is considered as a reference (illustrated in § 4.2).
 646 However, it cannot be used in routine to establish the complete heating distribution inside the core, due to the
 647 time required for reaching the temperatures equilibrium. Secondly, it is only applicable in upper part of the
 648 distribution where heating levels remain under around 4 W.g^{-1} , due to the maximum current intensity (2 A)
 649 applicable to heater wires. Nevertheless, as considered as the best approach of an absolute measurement, it
 650 enables to confirm results obtained by the calibration curve. In addition, the zero method is a way to study the
 651 loss of linearity as the heating rate increases. Therefore, an intensive use of this procedure was made during the
 652 2015 measurement campaign of CALMOS-2. Fig. 23 gathers 21 heating measurements obtained by both
 653 calibration and zero methods on the $0\text{-}4 \text{ W.g}^{-1}$ range. All measurements are obtained by the 4-wire technique
 654 leading to a very accurate power measurement (§ 4.2). Note that the zero method can require a significant
 655 measurement time because, close to the equilibrium, after each power adjustment we are dependent to the
 656 calorimeter time constant.

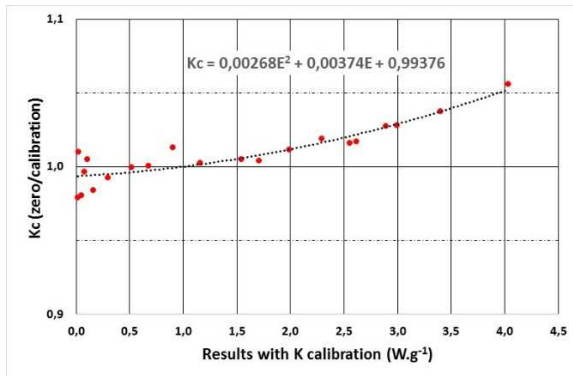
657 Fig. 23 gathers all results. The observed dispersion at very low heating rate (9 measurements under 700 mW.g^{-1}),
 658 is not considered as relevant. However, the figure shows that the discrepancy is within 2% up to around a 2.5
 659 W.g^{-1} heating range. Accounting experimental uncertainties (see § 16), we consider that no loss of linearity is
 660 highlighted and both methods are very close to each other up to that point. Beyond, the zero method provides
 661 values slightly higher than those obtained by calibration. That leads to a first experimental evaluation of the K_C
 662 correction factor to apply in equation (2), but limited to the $0\text{-}4 \text{ W.g}^{-1}$ range:

663

$$664 \quad K_C(E_T) \approx 0.00268 E_T^2 + 0.00374 E_T + 1 \quad (5)$$

665

666 Therefore, the correction is close to 4% at 3.5 W.g^{-1} and 5 % at 4 W.g^{-1} .



667

668

669 Fig. 23. Results discrepancy between “zero method” and “K calibration” methods up to a 4 W.g⁻¹ nuclear heating rate.

670

671 The remaining problem is evaluating the loss of linearity beyond 4 W.g⁻¹, i.e up to heating rates at the nominal
 672 power. That requires a reference measurement on which we can refer to follow accurately the proportional
 673 increase of the local power close to the calorimeter vicinity (see § 17.6).

674 14. Comparison between CALMOS and previous calorimeters

675 As any device in the core is loaded before the reactor start-up and withdrawn only after shutdown, it is
 676 impossible to compare two devices at the same location during the same cycle. Therefore, to qualify the
 677 transposition of the previous calorimeters geometry to the CALMOS one, the inter-comparison has been made in
 678 the excore area where insertion or removal of devices are allowed when the reactor is operating.

679 A first comparison was carried out in various excore locations with the second mock-up of CALMOS (very
 680 similar to the final geometry) and classical calorimeters. Table 4 shows the inter-comparison with a standard
 681 equipment (as described in Fig.1), made at three different locations and at the mid-plane.

682

Excore location	Calmos (2 nd mock-up)	Calor. N°30	Ratio (Calmos/N°30)

	(W/g)	(W/g)	
J1	1.22	1.14	1.07
H10	0.96	1.04	0.92
H9	1.90	1.67	1.14

683

684 Table. 4 – Comparison of a previous calorimeter (N°30) and the CALMOS mock-up in excore locations at the core mid-plane.

685

686 Despite some differences between measurement systems (aluminum alloys, external diameter, and gas
687 volume), this comparison shows a relative good agreement within 15 % for a heating up to 1.7 W.g⁻¹.

688 Nevertheless, this comparison must only retained as an indication.

689 A global comparison was made also for incore locations.

690

Incore location	Orientation	5-stage (W.g ⁻¹)	CALMOS (W.g ⁻¹)	Ratio (Calm/5-stage)
24 South	East	-	4.31	1.21
	West	3.55	-	
24 North	East	-	5.89	0.96
	West	6.12	-	
44	North-East	7.20	-	1.10
	South-West	-	7.90	
64 South	East	10.7	-	0.90
	West	-	9.60	

691

692 Table. 5 – Comparison between CALMOS-1 and the 5-stage calorimeter for incore locations.

693

694 Table 5 brings together some incore measurements, obtained by both the 5-stage calorimeter and CALMOS-1
695 along different cycles. Unfortunately, like in excore area, the comparison is only indicative:

- 696 - The reactor cycle is not the same, leading to a difference in the core loading,
697 - The location is the same, not the orientation,
698 - For 44 and 64 locations, measurements with CALMOS-1 are obtained just after the reactor start-up,
699 during the fast evolution of control rods,
700 - Finally, differences in terms of geometry between both calorimeters are significant, essentially the gas
701 volume and the presence of the external sheath for CALMOS-1.

702 For the three locations (24North, 44, and 64) the discrepancy does not exceed 10%, but is higher for the
703 24North location. Despite these differences, a relative good agreement is obtained between the two experimental
704 devices.

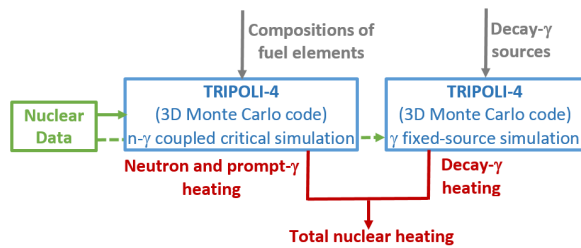
705 **15. Comparison with Monte Carlo calculations**

706 *15.1 Nuclear heating calculation scheme*

707

708 To evaluate the nuclear heating in devices irradiated in the OSIRIS reactor, a three-dimensional coupled
709 neutron-photon calculation scheme has been set up. The calculation scheme architecture is presented in Figure
710 24. It is based mainly on the TRIPOLI-4 Monte Carlo transport code [10, 14, 20, 22] which has been extensively
711 validated against experimental results from neutron flux measurements performed in ex-core and in-core
712 experiments [15, 18, 21]. As shown in Fig. 24, two-step TRIPOLI-4 simulations are needed to estimate the total
713 nuclear heating. The first one is a coupled neutron-photon critical simulation for the calculation of the nuclear
714 heating due to neutrons and prompt photons. The second one is a photon fixed- source simulation devoted for the
715 transport of the fission-product decay gammas. These two main steps need upcoming data: nuclear data which
716 represent the physics of simulations and irradiation data for setting up geometry and compositions of the core.
717 The calculation scheme uses nuclear data from the CEAV5_1.1 library, based mainly on the nuclear data library
718 JEFF3.1.1 [6].

719



720

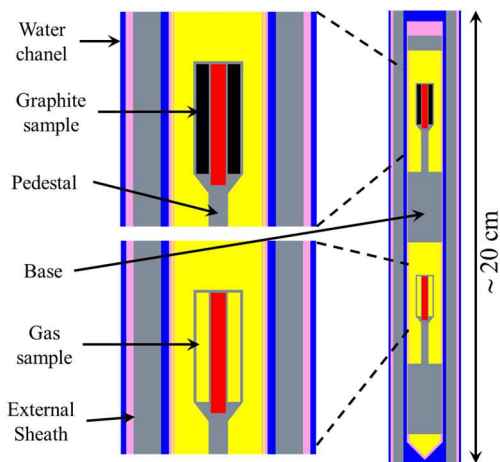
721 Fig. 24. Nuclear heating evaluation scheme architecture based on TRIPOLI-4 two-step neutron-photon simulations.

722

723 The user either gives irradiation data (control rods positions, loading of experimental devices...) or computes
 724 them by some deterministic calculation codes, in particular to obtain the isotopic compositions and the decay-
 725 gamma sources of the OSIRIS fuel elements.

726 The five-stage calorimeter (see Fig. 1) and the CALMOS-1 device were modelled thanks to the technical
 727 drawings as close as reasonably possible. Figures 25 and 26 show the axial and radial cross sections of the
 728 TRIPOLI-4 geometry modelling of the CALMOS device.

729

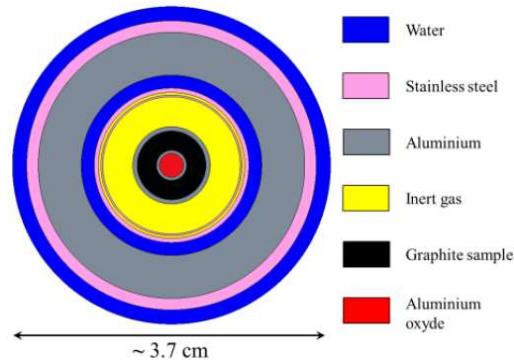


730

731

732 Fig. 25. Axial cross section of a TRIPOLI-4 modelling of the CALMOS-1 device

733



734

735

736 Fig. 26. Radial cross section of the TRIPOLI-4 geometry modelling of the CALMOS-1 device

737

738 The modelling of the OSIRIS core geometry is also as close as possible to technical drawings. Each fuel plate
 739 is modelled in the lattice, control rods can be modeled at their real axial position, and the axial discretization of
 740 fuel element compositions can be modified.

741 To ensure Monte Carlo standard deviations less than 1% for all calculated tallies (for fluxes or nuclear heating
 742 for neutrons, prompt and decay photons), each TRIPOLI-4 simulation was carried out using one hundred
 743 processors during about ten days.

744

745 *15.2 Results*

746

747 Several comparisons between calculations and measurements were performed with the five-stage calorimeter
 748 and the CALMOS-1 experimental device when irradiated in different positions and during different cycles of the
 749 OSIRIS reactor.

750

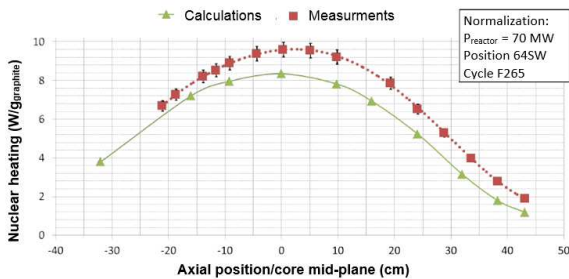
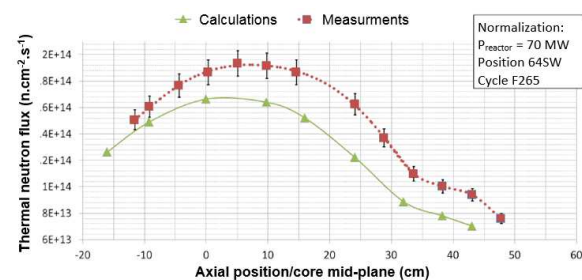


Fig. 27. Axial profile of nuclear heating: calculation-measurement comparison for the CALMOS-1 device (64SW location, cycle F265)



754
755 Fig. 28 Axial profile of the thermal neutron flux: calculation-measurement comparison for the CALMOS-1 device (64SW location, F265
756 cycle).

757
758 Figures 27 and 28 show examples of typical calculated and measured axial profiles of nuclear heating (in the
759 graphite sample) and thermal neutron flux (at the rhodium SPND location) for the CALMOS-1 device.

760 Results shown in these figures correspond to the F265 cycle and the 64 South-West experimental location,
761 normalized at the 70MW rated power.

762 Globally, we have good consistency between axial profiles of nuclear heating and thermal neutron flux
763 obtained both by calculations and by measurements. However, calculated values systematically underestimate
764 those measured. Discrepancies between calculation and measurements are about -15% at the core mid-plane
765 level. According to measurement uncertainties (see §16), we can consider that the calculated values are close to
766 measurement results within 2σ of measurement. A first possible reason of the observed discrepancies between
767 experiments and simulations could be the lack of knowledge of the exact composition of the fuel elements
768 (determined by preliminary calculations). Another assumption could be a lack in terms of photon production
769 nuclear data. The use of recent nuclear data evaluations such JEFF3.3 or ENDF/B-VIII will be investigated.

770 The nuclear heating calculation scheme is a useful tool for analysis and understanding. That allowed
771 quantifying a "geometric effect" of 6% in terms of measured nuclear heating, between the five-stage calorimeter
772 and CALMOS, when both devices are irradiated exactly in the same incore position.

773 Measurements performed by the two calorimeters cannot really be directly compared. This would have
774 required identical irradiation conditions in a same core i.e in terms of core loading and control rods positions (see
775 §14 and Table 5). Therefore, the simulation can be here a good help to perform a fully relevant comparison.

776 In addition, with the presented calculation scheme, we have access at each component taking part in the
777 nuclear heating in the samples: Neutron energy deposition (about 15%), prompt photon energy deposition (about
778 65%), and decay photon energy deposition (about 20%). The most part of nuclear heating being due to photons
779 (about 85 %). The contribution of neutrons (essentially fast neutrons above 1 MeV) is not negligible.

780

781 **16. Uncertainties evaluation**782 *16.1 Nuclear heating measurement*

783

784 Uncertainties associated to nuclear heating measurements are established when the preliminary calibration (2)
785 is used in routine to perform the measurement (use of the K coefficient). However, such evaluation is made
786 accurately only for the 0-4 W.g⁻¹ heating range, for which the zero method could be taken as reference. In that
787 range, the K_C coefficient defining the loss of linearity could be evaluated quite precisely thanks to the 4-wire
788 technique measurement (§ 13). We can consider that the K calibration, the $\Delta\Delta T$ temperature difference and the
789 K_C correction coefficient of (2) are independent:

- 790 - The uncertainty associated to K depends on the cell slopes determination made during the preliminary
791 calibration (°C.W⁻¹). It is evaluated at 3.8 % at one standard deviation (1 σ) and is independent of the heating
792 level,
- 793 - The $\Delta\Delta T$ value comes from the measurement of four temperatures. The uncertainty of each thermocouple
794 (calibration certificate) and those coming from the temperature measurement device, lead to total
795 uncertainties decreasing with $\Delta\Delta T$ rise: 12 % for 5 °C, 5.5 % for 11 °C and 1.9 % for 42 °C $\Delta\Delta T$ (1 σ),
- 796 - K_C is evaluated thanks to the zero method and the CAST3M Finite Element Model [28]. The only
797 experimental process is kept in the present evaluation. Despite of the low measurements we could perform in
798 the core, obtained points fit well with the K_C curve in Fig. 23. An analytical approach allows assessing for
799 K_C a global uncertainty to 2 % (1 σ).

800

801

Heating W.g ⁻¹ (graphite)	0.5	1	2	4
σ_{E_T/E_T} at 1 σ (%)	12.7	7.0	5.4	4.7

802

803 Table 6 – Uncertainties on heating measurements when deduced from the calibration and up to a 4 W.g⁻¹ heating rate

804

805 Therefore, if the measurement is made with the preliminary calibration and within a 0 to 4 W.g⁻¹ range, expected
 806 uncertainties are those of Table 6, as a function of the heating rate. Beyond a 4 W.g⁻¹ heating rate, the number of
 807 available measurements did not allow to assess the definitive associated uncertainty. However, it is expected to be no
 808 less than 15 % (1 σ) at 12 W.g⁻¹.

809

810 *16.2 Conventional thermal neutron flux*

811

812 Measurement of the thermal neutron flux thanks to the specific rhodium SPND requires to suppress the epithermal
 813 response of the emitter (See § 7). That is the preliminary step to deduce the thermal neutron flux from the measured
 814 current. Therefore, the axial distribution of the epithermal flux/thermal flux ratio has been calculated by the TRIPOLI-
 815 4 Monte Carlo for the four typical experimental locations inside the core, i.e 24South, 24North, 44, and 64 (sub-
 816 locations for central 44 and 64 locations do not need to be distinguished in terms of spectra). The epithermal index
 817 was calculated for all accessible altitudes with the calorimeter taking into account the real geometry (sensor + cooling
 818 water layers + external sheath), the rods position and the actual core loading. Therefore, the following terms are taken
 819 into account for the uncertainty evaluation:

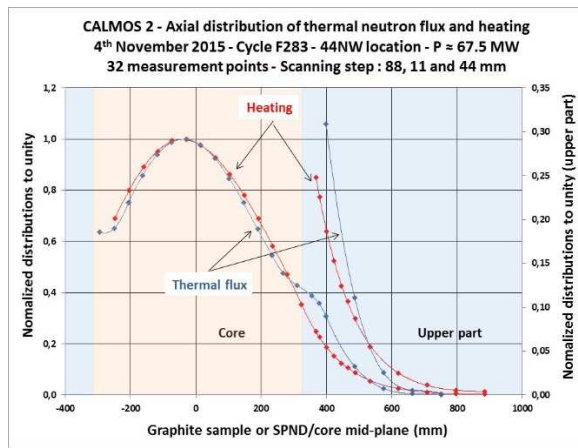
- 820 - The calculated epithermal index by TRIPOLI4,
- 821 - The thermal sensitivity of the rhodium SPND,
- 822 - The measured intensity delivered by the SPND.

823 Finally, the global uncertainty associated to the conventional thermal flux measurement by this rhodium SPND, in
 824 CALMOS-2 configuration, is 8 % at 1 σ [17].

825 17. Characterization of the OSIRIS incore radiation field thanks to CALMOS devices

826 17.1 Comparison of heating and thermal flux profiles in the core

827
 828 The probe allows measuring separately the nuclear heating, the thermal neutron flux or both at the same time.
 829 Fig. 29 shows an example with 32 simultaneous measurement points, heating and thermal flux, performed in the
 830 44NorthWest location during the F283 cycle with CALMOS-2, which allows observing behaviors of both
 831 quantities along the scanning height (distributions normalized to unity).



832
 833
 834 Fig.29 – Simultaneous measurement of heating and thermal neutron flux in the 44North-East location. Values are normalized to unity.

835
 836 Fig. 29 shows that in the middle part of the core, distributions of heating and neutron flux have roughly the
 837 same shape. However, differences of behavior are measured above:

- 838 - At the core-moderator transition area centered around +320 mm/mid-plane, we observe a significant rise
- 839 of thermal neutron flux (slope break), whereas this transition has no effect on the nuclear heating
- 840 evolution,

841 - Above the core (zoomed part on right scale of Fig. 29) the heating attenuation is quite different from the
 842 thermal flux one. The thermal flux decreases faster than the heating, with a measured ratio of 2 each 40
 843 mm against 80 mm for heating.

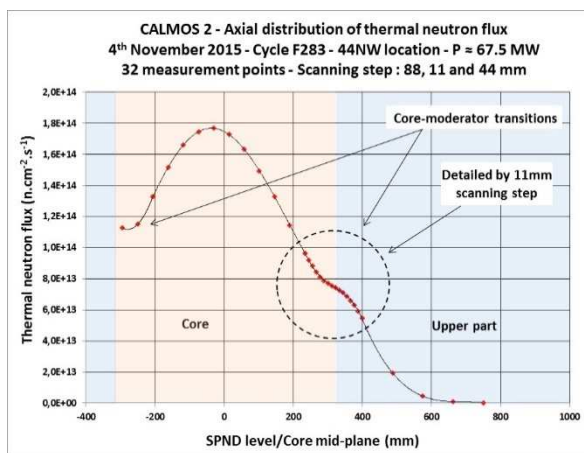
844

845 *17.2 Fine analysis of thermal neutron flux behavior at the core-moderator transition*

846

847 Fig. 30, which relates to the only thermal flux in absolute values, shows the possibilities offered by the HMI
 848 automatic displacement system, allowing to refine deeply the obtained profiles for given areas in the total stroke. At
 849 the core-moderator transitions (here in the upper part around +320 mm/mid-plane), the scan step has been reduced to
 850 the 11 mm minimum value, detailing the slope break in the thermal flux evolution.

851



852

853

854 Fig.30 – Measurement of the thermal neutron flux in the 44 North-East location. Detail of the distribution at the core-moderator transition.

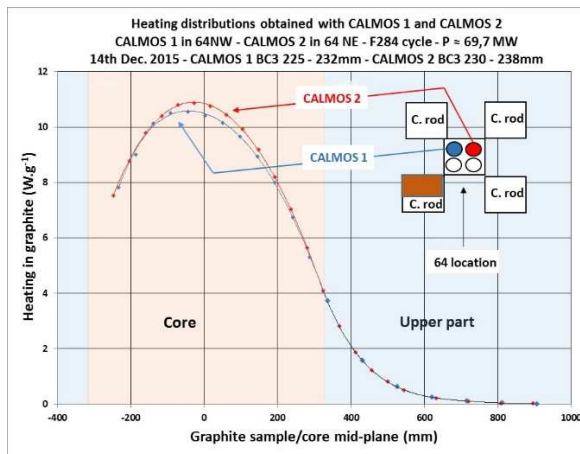
855

856 *17.3 Checking of consistency between both CALMOS devices responses*

857

858 To check the consistency between CALMOS-1 and CALMOS-2 prototypes, both devices were loaded side-
 859 by-side (37 mm distance) in the two north positions of the 64 location during the F284 cycle (Fig. 31).
 860 Distributions of nuclear heating and thermal neutron flux were obtained with each device, but operated
 861 separately, to avoid any influence on each other. During the scans, made at the 70 MWth nominal power, among
 862 the four control rods surrounding the location, only BC3 (in brown) in the south part of the core is in operation
 863 and moving in the lower part of its stroke. Such configuration allows approximating same irradiation conditions
 864 in north part of the 64 location. Fig. 31 illustrates also the CALMOS configuration with regard to the control rod
 865 in operation.

866 Fig. 31 shows that heating profiles are almost identical, with a slight discrepancy in the mid-plane region in
 867 which the CALMOS-2 signal (red curve) is around 3 % higher.
 868



869

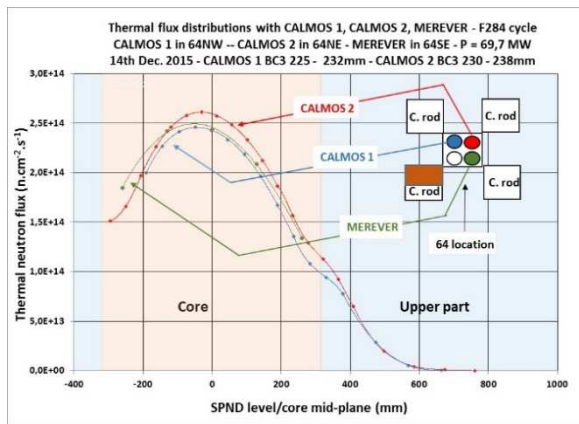
870

871 Fig. 31 – Distributions of nuclear heating obtained with both prototypes located in the 64 North location

872

873 Such results show that both devices give coherent responses in spite of a significant difference between
 874 sensitivities (K calibration discrepancy is 16.6 % between each other).

875



876

877

878 Fig. 32 – Distributions of the thermal neutron flux obtained in 64 location with CALMOS-1 (blue) CALMOS-2 (red) and the MEREVER device
879 (green) equipped with standard rhodium SPNDs

880

881 The comparison made for the thermal neutron flux is illustrated in Fig. 32. At mid-plane, measurements by
882 CALMOS-2 (red curve) are also higher around 6 % than CALMOS-1 (blue curve). However, conversely to the
883 heating, we note a thermal flux in CALMOS-1 remaining lower even in the fissile-moderator transition (brown-
884 blue transition on Fig. 32).

885 In addition, a static device called MEREVER is located also in the same 64SE location (in green). Used for
886 many years in the OSIRIS reactor for thermal flux measurements and qualified, it is instrumented with 10
887 rhodium standard SPNDs (50 mm emitter length) inside an aluminum rod and allows to plot the flux profile with
888 5 axial measurements points covering +/-260 mm/mid-plane. In comparison with those obtained with CALMOS
889 devices, we observe that profiles are very similar, except for low altitudes under the mid-plane (green curve),
890 demonstrating that the thermal neutron flux at the MEREVER position is influenced by the rod position, closer to
891 this device.

892 The global consistency in thermal flux measurement found between CALMOS and MEREVER devices, shows
893 that the 10mm short emitter SPND, especially developed for the CALMOS program, is qualified.

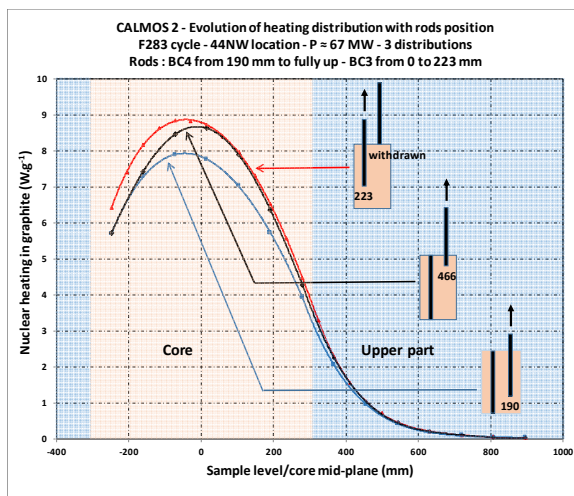
894

895 *17.4 Surveillance of the heating evolution during a reactor cycle*

896

897 To follow the evolution of the heating distribution along the entire reactor F283 cycle, the CALMOS-2 device
 898 is placed inside the 44North-West location. Eight different scans are successively performed (reactor power
 899 unchanged), spread from the beginning of the cycle to the reactor shutdown.

900



901

902

903 Fig. 33 – Follow-up during the whole F283 reactor cycle of the nuclear heating distribution obtained with the CALMOS-2 device placed in the 44
 904 North-West location. Three distributions corresponding to three representative control rods positions along the cycle.

905

906 The three most relevant distributions obtained are plotted in Fig. 33, well representative of the whole control
 907 rods evolution during the cycle going from the position “rods inserted” (blue curve) to the rods position at
 908 shutdown time, with one rod completely extracted (red curve).

909 The complete recording along the cycle permits to measure at this location, not only a 12 % increase of the
 910 heating rate at the core mid-plane, but also to observe and to measure the axial displacement of the position of the
 911 maximum flux plane (moving from -40 mm, 0 and moving down again -40 mm/MP at shutdown time).

912 Such information is of major importance to predict the total heat deposition in any experimental device in the
913 core.

914

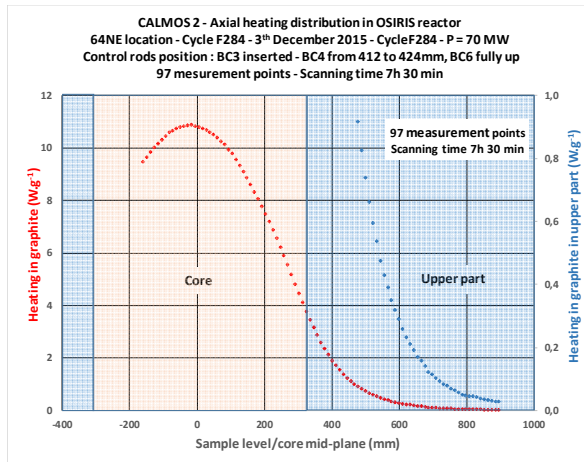
915 *17.5 Heating distribution with very high definition*

916

917 To measure a relevant distribution in the core (heating or neutron flux), the control rods axial displacement
918 (rise movement) must be very short during the whole scan duration, i.e involving a negligible effect on measured
919 distributions. That can be the case only at mid-cycle, because rods are in the middle of their mechanical stroke,
920 therefore at their maximum efficiency. Fig. 34 shows an example of a complete scanning, covering the whole
921 calorimeter stroke, performed with the 11 mm minimum scanning step, offering the best definition. Taking into
922 account the time response of the calorimeter (2min 30s), added to the time required to move the probe, the total
923 measurement time is 4min 30s per point. A 7 h 30 min scanning time is required to perform the 97 measurement
924 points necessary to cover the whole calorimeter stroke. That shows the ability of such calorimeter, thanks to the
925 automatic displacement system, to refine the profile definition as deeply as necessary.

926 Obviously, the measurement is a compromise between the definition and the acceptable scanning time. To
927 keep relevant, the modification of the radiation field must be considered as negligible over the total time required
928 to draw its distribution.

929



930

931

932 Fig. 34. Test of the highest definition. Nuclear heating distribution in the 64North-Esat location during the F284 cycle. The whole scanning height is
 933 covered by 97 measurements points for a total scanning time of 7 hr 30 min.

934

935 17.6 Reactor start-up monitoring

936

937 For monitoring the complete divergence of the reactor during the F284 cycle, the CALMOS-2 calorimeter
 938 (sample cell) is placed at the core mid-plane altitude before start-up. The 64-water box loading is as described in
 939 Figs. 31 and 32, with CALMOS-2 in 64North-East and the MEREVER device in 64South-Est location, with only
 940 a 37 mm distance between both devices. During the reactor power rise, from the divergence to nominal power,
 941 the only two BC6 and BC4 control rods are operating. Other rods are either fully up or fully inserted i.e without
 942 any effect on the axial heating distribution. Relative positions between these two rods and devices appear in Fig.
 943 32.

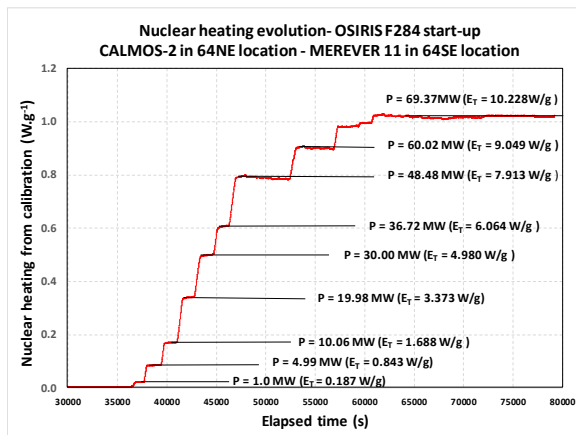
944 Among the ten rhodium SPNDs inside the MEREVER device, two SPNDs (N°5 and N°6) are side by side and
 945 exactly at the core mid-plane i.e very close to the sample cell of the calorimeter. During the power rise, we can
 946 make the following assumptions regarding positions of the sample cell and that of these two SPNDs:

- 947 - During the power rise, up to around 50 MW, first the BC6 rod is moving up in the upper part of its stroke
 948 between 430 and 550 mm, i.e in an area clearly above the mid-plane. Then, the second rod is moving up in
 949 the lower part of its stroke, from 50 MW to nominal power, between 0 and 170 mm i.e clearly under the
 950 mid-plane. These two areas are far away enough from the core mid-plane vicinity to consider that, in a
 951 first approach, there is no significant effect on the flux gradient between 64NE and 64SE positions,
 952 - As there is no change of environment at the mid-plane vicinity (control rods in operation, static position of
 953 the CALMOS calorimeter), the spectrum does not change with reactor power i.e the gamma spectrum, the
 954 neutron spectrum and the ratio among them remain unchanged.

955

956 Such situation allows assuming, and that was the researched objective, that the nuclear heating (CALMOS-2
 957 monitoring) and the thermal neutron flux (MEREVER monitoring) follow the same relative evolution from the
 958 divergence to the nominal power. Therefore, signals recorded from N°5 and N°6 SPNDs of the MEREVER
 959 device can be taken as reference to monitor the calorimeter linearity from 0 to 70 MW.

960



961

962

963 Fig. 35- CALMOS-2 in 64North-East location: Recording of nuclear heating evolution along the F284 reactor start-up from 0 to 69.37 MW. The
 964 MEREVER device is in 64South-East location. The reactor power rise is made with 9 steps allowing the recording of stabilized signals.

965

966 Fig. 35 shows the evolution of the measured heating (deduced from the calibration) with the CALMOS-2
 967 calorimeter along the whole F284 OSIRIS divergence. Nine steps during the power rise allow to record stabilized
 968 signals of the calorimeter and those provided by SPNDs.

969 The results processing allows deducing a second estimation of the linearity loss for heating measurements up to the
 970 nominal power. To do it, the heating measured at 5 MW is taken as reference then, all other measurements are
 971 recalibrated thanks to the relative evolution of MEREVER SPNDs. We note that the obtained correction is identical
 972 whatever the SPND taken as reference (N°5 or N°6). Fig. 36 shows the deduced experimental evolution of $K_C(E_T)$
 973 (ratio between recalibrated and measured values) between 0 and 70 MW i.e covering the 0 to 11 $W.g^{-1}$ heating range:

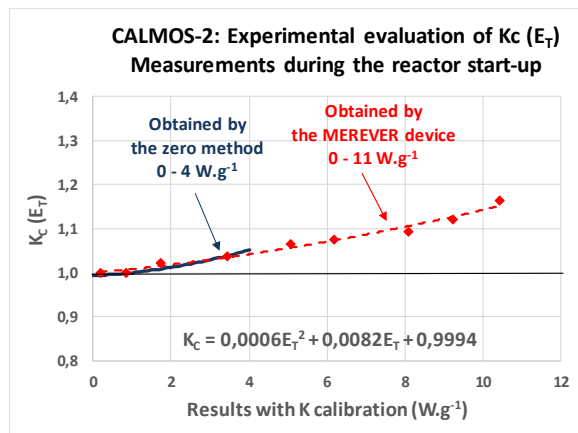
974

$$975 \quad K_C(E_T) \approx 0.0006 E_T^2 + 0.0082 E_T + 1 \quad (6)$$

976

977 Results show that the correction is not negligible and close to 10 % at 8 W/g and close to 14 % at 10 $W.g^{-1}$.

978



979

980

981 Fig. 36 – CALMOS-2 at the core mid-plane in the 64North-East location: Loss of linearity up to the nominal power during the F284 OSIRIS start-
 982 up. Recalibration of heating measurements thanks to the MEREVER rodium SPNDs in close vicinity.

983

984 On the same figure are plotted also, the first experimental evaluation of $K_C (E_T)$ deduced from the zero method
985 comparison (see § 12). Fig. 36 shows that the trend previously obtained, for the correction coefficient limited to a
986 0-4 W/g heating range, is in correct agreement with these latest measurements.

987 To reinforce such result, the processing of measured heating levels has been made also with the reactor power
988 taken as reference. In that case, we need to consider that any variation of the reactor global power involves a
989 same relative variation of the local power at the mid-plane vicinity. The same trend is obtained with a correction
990 close to 14 % at 10.4 W.g⁻¹ against 15 % found in Fig. 36. Therefore, for nuclear heating measurements obtained
991 from the calibration in CALMOS-2, the K_C expression of (6) is applied.

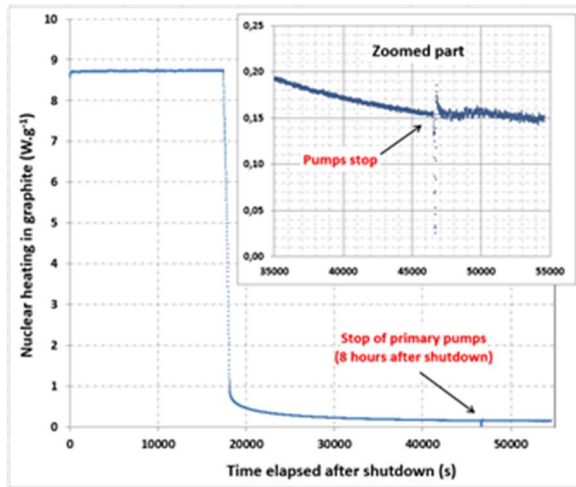
992

993 *17.7 Recording of the residual power decay after shutdown*

994

995 The CALMOS calorimeter has been tested also to follow the residual power decay after the reactor shutdown.
996 Fig. 37 shows a 10 hours recording performed after shutdown at the end of the F283 cycle. Just after shutdown,
997 the residual power drops sharply to almost 10% of the nominal value, before decreasing more slowly. After an 8
998 hours elapsed time, the measured $\Delta\Delta T$ is only 1.63 °C leading to a residual heating level to around 150 mW.g⁻¹.
999 At this time, the reactor procedure requires to stop the primary pumps, involving a change of cooling conditions
1000 for the calorimeter, switching from the forced convection to the natural convection regime.

1001



1002

1003

1004 Fig. 37 – Decay of the residual power after the end of the F283 OSIRIS cycle. Recording during 10 hours after shutdown. The signal behaviour
 1005 before and after the change of cooling regime appears in the zoomed part (upper right corner).

1006

1007 The zoomed part in Fig. 37 (upper right corner) shows that the signal is disturbed at the pump stop and the noise
 1008 becomes stronger in natural convection. However, the signal decay is still coherent because, after this event, it follows
 1009 the same slope of decay, demonstrating that the calorimeter remains reliable even in natural convection regime,
 1010 established inside the water gap between the calorimetric probe and the internal surface of the sleeve. This result is of
 1011 major importance because that shows that the CALMOS calorimeter keeps its ability to monitor the residual power
 1012 independently of OSIRIS thermohydraulic conditions.

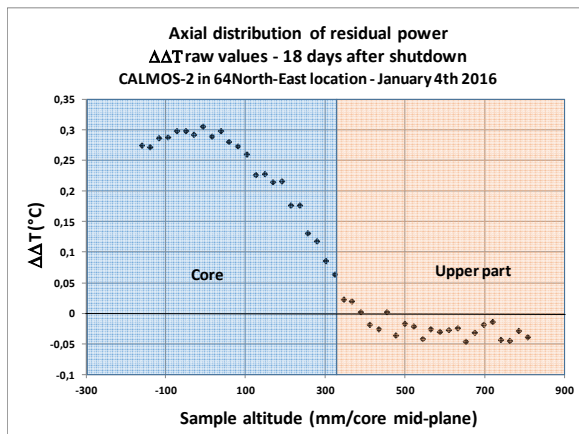
1013

1014 *17.8 Establishment of the core residual power distribution 18 days after shutdown*

1015

1016 At the end of the F284 cycle, the monitoring of the power residual decay was extended up to 18 days after the
 1017 reactor shutdown. At this time, when the CALMOS probe is located at the core mid-plane, the measured $\Delta\Delta T$ is
 1018 reduced to 0.31 °C leading to a nuclear heating rate of about 29 mW.g⁻¹ (C).

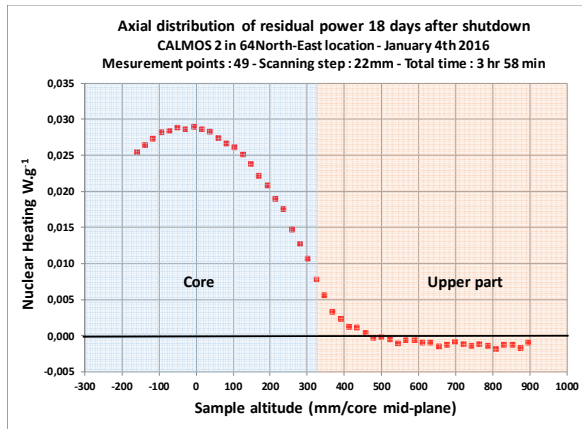
1019 Despite this very low signal, a scanning is attempted to establish the axial distribution of the residual power in
1020 the core, in 64North-East location, with a step reduced to 22 mm and a 5 min measurement time at each altitude.
1021 Fig. 38 shows the obtained recording of $\Delta\Delta T$ raw values. Despite some discrepancies, the nuclear heating
1022 distribution is still coherent and measurable.
1023



1024
1025
1026 Fig. 38 – Axial distribution of raw $\Delta\Delta T$ values of the CALMOS-2 calorimeter, in the 64NE experimental location, 18 days after shutdown of the
1027 F284 OSIRIS cycle.
1028

1029 We remind that the study of the calorimetric cell response shows clearly that, even though $\Delta\Delta T$ is the only
1030 quantity well representative of nuclear heating, the relative distribution can be deduced from each cell ΔT as
1031 demonstrated in Fig. 22. Taking advantage of this property, for plotting the complete curve of the final residual
1032 power in the core, we retain only the absolute measurement of heating at the core mid-plane. Then, the rest of the
1033 distribution is deduced from the relative response of the “ Δt sample” showing a much weaker dispersion. Results
1034 appear in Fig.39.

1035



1036

1037

1038 Fig. 39 – Axial distribution of the core residual power, plotted by the CALMOS-2 measurement device 18 days after shutdown of the OSIRIS F284
 1039 cycle.

1040

1041 That demonstrates that it is of prior importance, during the manufacturing, to choose the thermocouples
 1042 accurately to enable the very low ΔT measurements. They must provide the lowest dispersion as possible in a
 1043 same temperature field (importance of preliminary calibration). Each thermocouple embedded in the cell base
 1044 (“cold temperature”) is calibrated with two reference points, melting ice and boiling of water, whereas each
 1045 thermocouple embedded in the pedestal (“hot temperature”) is calibrated with four references, boiling of water
 1046 and melting points of Tin (232 °C), Lead (327 °C), and Zinc (420 °C). After selection, the lower the dispersion is,
 1047 the lower the required correction is (or negligible) for very low heating rates. For the four thermocouples of the
 1048 CALMOS-2 calorimetric cell, the preselection led to a very low discrepancy among them, measured to 0.2 °C
 1049 over the 420 °C total range of the calibration.

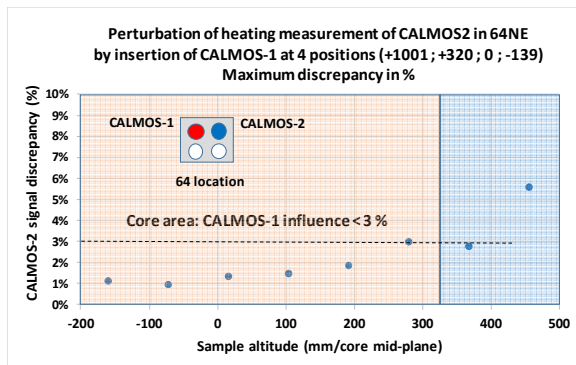
1050 Obtained results show the ability of the CALMOS device to establish the nuclear heating distribution in the
 1051 core, from the nominal power up to after 18 days of cooling time after shutdown. Therefore, we can consider that
 1052 the calorimetric cell offers 3-decade dynamic range.

1053 **18. Mutual perturbation between the two CALMOS devices in a same experimental location**

1054 Inside an experimental reactor, it is essential to check that the measurement we are performing is relevant. That
 1055 requires checking that any potential modification in the environment (control rod, experimental device...) does
 1056 not affect significantly the radiation field we are measuring. That is the case if we want to use the two CALMOS
 1057 devices in the same water box to characterize the same location. Moving down or moving up the mobile
 1058 equipment of a system along its main axis can disturb the other one.

1059 During the last F284 cycle, CALMOS-1 and CALMOS-2 were placed side-by-side, respectively in the
 1060 64North-West and the 64 North-East locations of the core.

1061

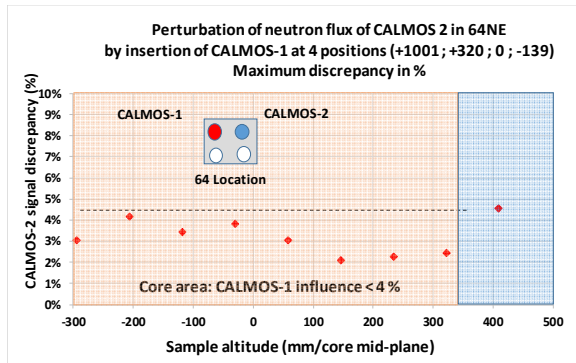


1062

1063

1064 Fig. 40 – CALMOS-2: Discrepancy in nuclear heating measurement among the 4 measurements corresponding to the 4 positions of the CALMOS-1
 1065 probe insertion in the core.

1066



1067

1068

1069 Fig. 41 – CALMOS-2: Discrepancy in thermal neutron flux measurement among 4 measurements corresponding to 4 positions of the CALMOS-1
 1070 probe insertion in the core.

1071

1072 Four successive complete scanning were performed with CALMOS-2 (nuclear heating + neutron flux
 1073 measurements, 88mm scan step each) for four fixed positions of the CALMOS-1 calorimetric probe,
 1074 corresponding to the rest position (+1001mm), the entrance of the core (+320 mm), the core mid-plane (0mm),
 1075 and at the bottom (-139 mm). These four positions are representative of the potential perturbation.

1076 Figs. 40 and 41 gather all maximum measured discrepancies, evaluated at eight altitudes of CALMOS-2
 1077 calorimeter, for both heating and neutron flux measurements. Results show that, inside the core, the maximum
 1078 perturbation involved by the presence of the CALMOS-1 probe in CALMOS-2 vicinity remains very low,
 1079 respectively less than 3 % for heating measurement and less than 4% for the thermal neutron flux. Considering
 1080 experimental uncertainties, such results led us to assume that, in first approximation, any scanning performed by
 1081 one displacement system does not disturb the measurements acquisition carried out by any other similar device,
 1082 for both nuclear heating or for thermal neutron flux measurements. Both devices can work together
 1083 independently.

1084 **19. Conclusion**

1085 From the first idea in 2002 to the completion of a real qualified measurement prototype suited to an MTR
1086 reactor, followed by the comprehensive analysis of obtained results, the CALMOS R&D program took place over
1087 a period of 15 years. The development and the qualification of the whole measurement system required a
1088 succession of thermohydraulic, neutron, and mechanical studies. Among them, the modelling of the calorimetric
1089 probe, answering to OSIRIS incore thermohydraulic conditions, permitted to design a cell geometry well suited to
1090 nuclear heating rates inside the core. Two mock-ups tested in the excore area allowed to validate the
1091 measurement protocol for this innovative superimposed geometry. Then, the transposition to incore
1092 measurements needed the development of a specific displacement system to obtain axial nuclear heating
1093 distributions inside the core while ensuring the cooling conditions of the probe and matching with OSIRIS safety
1094 requirements. The whole measurement campaign in real incore conditions by both CALMOS devices ran from
1095 2013 to 2015, covering 11 reactor cycles, around 22 days each.

1096 About the calorimetric probe working, the main results are as follows:

- 1097 - Using the zero method, almost independent of the calibration phase, allows reducing the number of
1098 assumptions in the heating measurement process. The most important improvement brought in the last
1099 version is the implementation of the 4-wire technique in the reference cell, which allows suppressing any
1100 assumption about the heater element ageing. That enables to reduce the associated uncertainty to heating
1101 measurements at 4.7 % at 1σ for a $4 \text{ W.g}^{-1} (\text{C})$ heating rate,
- 1102 - The entire absolute axial distribution in the core can be obtained by performing a single absolute
1103 measurement at a given altitude, the rest of the curve is deduced thanks to the relative response of any of
1104 the cells,
- 1105 - The zero method is used as a reference measurement for the probe non-linearity assessment.
1106 Determination of the cells slope in $^{\circ}\text{C.W}^{-1}$ shows that the response is almost linear within a $0\text{-}5 \text{ W.g}^{-1}$
1107 heating range, with a measured discrepancy not exceeding 4 %,

1108 - The global sensitivity has around a 3-decade dynamic range, offering the possibility not only to follow the
1109 core residual power up to 2 weeks after shutdown, but also after this cooling time to draw its axial
1110 distribution.

1111
1112 The CALMOS-1 device has been tested during ten reactor cycles. Despite the short irradiation campaign of
1113 the CALMOS-2 upgraded version, carried out during the last three cycles of the OSIRIS reactor due to its final
1114 shutdown scheduled in December 2015, many tests were performed in different core conditions. That highlighted
1115 the various possibilities offered by the new displacement system when associated with the complete automatic
1116 driving system to characterize the incore radiation field. Among major results, we note:

- 1117 - The automatic probe mobility, programmed through a Human Machine Interface thanks to a specific
1118 software, allows obtaining very well defined profiles both for nuclear heating and for thermal neutron flux
1119 measurements. The scanning step and partial and/or total measurement times can be adjusted as required,
1120 focused on given target regions and to the reactor conditions in order to keep a relevant measurement with
1121 regard to the control rods evolution,
- 1122 - The programming of measurement sequences helps a lot in monitoring the radiation field evolution
1123 throughout the reactor cycle, because it can be adapted to reactor conditions,
- 1124 - For the most critical situation, a CALMOS device closer as possible to the control rod in operation, the
1125 complete withdrawal of the mobile equipment from its external sheath induces a 45 pcm positive reactivity
1126 on the core. Therefore, the adopted displacement speed of 1 mm.s^{-1} in the core involves a reactivity effect
1127 less than 0.1 pcm.s^{-1} , fully compatible with reactor control rules.

1128
1129 However, the global feedback of the CALMOS program leads us to some improvement perspectives. In that
1130 program, the main purpose was to obtain a calorimeter answering to a very large nuclear heating range, ranging
1131 from 13 W.g^{-1} at the core mid-plane at nominal power to the residual heating at 1 m above the core. Therefore,
1132 the sensitivity was a compromise. It must be high enough for a measureable $\Delta\Delta T$ in the lower part of the heating

1133 range, but sufficiently low at high level to limit absolute temperatures in the cell, because leading to heat losses
1134 by radiation and conduction in gas. Therefore, in the upper heating range, the loss of the linearity is significant.
1135 So, as main prospect, another design would be optimizing the geometry so as to limit the sensitivity, therefore the
1136 maximum temperature of inner walls inside the cell, to suppress as drastically as possible heat losses by radiation,
1137 which are very difficult to assess by calculation and to suppress in the design.

1138 Secondly, even though it cannot be used in routine for establishing any axial distribution, results showed the
1139 importance of the zero method, considered as the best approach of an absolute measurement. That leads to the
1140 second major improvement, which would be to design a heater element able to simulate the energy deposit up to
1141 highest heating levels in the core, to perform an absolute measurement for assessing more accurately the loss of
1142 linearity when using the calibration coefficient.

1143 The intensive use of CALMOS-2 in the core, cumulating a total 70 hours automatic scanning time, has
1144 demonstrated its reliability for OSIRIS in-core conditions up to a 12 W.g^{-1} heating rate and up to a 2.5×10^{14}
1145 $\text{n.cm}^{-2}.\text{s}^{-1}$ thermal neutron flux. While meeting the reactor safety requirements, the CALMOS device becomes an
1146 operational equipment suited to the surveillance and the qualification of the incore radiation field in an MTR
1147 reactor, a key data for the dimensioning and the surveillance of any experimental device irradiated inside.

1148 **Acknowledgments**

1149 This R&D program was carried out in the framework and with the financial support of the MCIS/INSNU
1150 project of CEA/DEN. Authors wish to thank the DEN/DER/SPESI and SRJH services of CEA/Cadarache for
1151 their support, and the LIMMEX joint laboratory between CEA and Aix-Marseille University for fruitful and
1152 constructive discussions along this R&D program.

1153 The constant support of the OSIRIS operating personnel from CEA/DEN at the Saclay center was crucial for
1154 performing irradiation campaigns inside the reactor.

1155 Finally, authors wish to address special thanks to Valérie Lepeltier, Véronique Clouté-Cazalaa and Jean-Marie
1156 Guyot, Romain Illiaquer, Eric Bouard, Jacques Bubendorff and Cedric Courteaux from the CEA/DEN of the

1157 Saclay center for their help through their respective specialties, without which we could not have conducted this
1158 research program.

1159

1160

1161

1162

1163

1164 **References**

- 1165 [1] F. Ayela, H. Derrien “The development of an electrically compensated differential calorimeter for the measurement of in-pile heat
1166 evolution”. Technical Report CEA-R-2190, 1962.
- 1167 [2] IAEA, “International Intercomparison of Calorimeters”, Report N° 128, 1970.
- 1168 [3] M.S. Kim, S.Y. Hwang, H.S. Jung, and K.H. Lee, “Measurements of Nuclear Heating Rate and Neutron Flux in HANARO CN Hole for
1169 Designing the moderator cell of cold neutron source.” Korea Atomic Energy Research Institute. Proceedings of IGORR, (2005).
- 1170 [4] H. Carcreff, A. Alberman, L. Barbot, F. Rozenblum, D. Beretz and Y. K. Lee, “Dosimetry Requirements for Pressure Vessel Steels
1171 Toughness Curve in the Ductile to Brittle Range”, J. of ASTM International (JAI), Vol. 3, Issue 3, (Mar., 2006).
- 1172 [5] Y.K. Lee and F. Malouch, “Analysis of OSIRIS In-Core Surveillance Dosimetry for GONDOLE Steel Irradiation Program by Using
1173 TRIPOLI-4 Monte Carlo Code”, 13th International Symposium on Reactor Dosimetry (ISR13), Akersloot, Netherlands, May 21-25,
1174 2008.
- 1175 [6] Santamarina A., Bernard D., Blaise P., Coste M., Courcelle A., Huynh T.D., Jouanne C., Leconte P., Litaize O., Mengelle S., Noguère
1176 G., Ruggieri J.M., Sérot O., Tommasi J., Vaglio-Gaudard C., Vidal J-F., “The JEFF-3.1.1 Nuclear Data Library, JEFF Report 22,
1177 Validation Results from JEF-2.2 to JEFF-3.1.1,” NEA No. 6807, OECD/NEA Edition 2009.
- 1178 [7] H. Carcreff, Patent N° FR 1060068, December 3, 2010.
- 1179 [8] H. Carcreff, “CALMOS : Innovative device for the measurement of nuclear heating in material testing reactors”. Journal of ASTM
1180 International (JAI , Volume 9, Issue3, March 2012.
- 1181 [9] H. Carcreff, V. Clouté-Cazalaa, and L. Salmon, “Development, calibration and experimental results obtained with the innovative
1182 calorimeter (CALMOS) for nuclear heating measurements”, IEEE Trans. Nucl. Sci.,vol.54, no.4, pp. 1369-1376, Aug.2012.

- 1183 [10] F. Malouch, "Development and Experimental Validation of a Calculation Scheme for Nuclear Heating Evaluation in the Core of the
1184 OSIRIS Material Testing Reactor". Journal of ASTM International (JAI), Volume 9, Issue 4, April 2012.
- 1185 [11] J. Brun, and coll, "Numerical and Experimental Calibration of a Calorimetric Sample Cell Dedicated to Nuclear Heating Measurements",
1186 IEEE Transactions on Nuclear Science, Vol.59, N°.6, Dec 2012.
- 1187 [12] F. Lopez "Calculs d'indice épithermique dans le dispositif CALMOS pour m'interprétation du signal collectron dans et au-dessus du
1188 coeur du réacteur OSIRIS" note CEA/DEN/DM2S/SERMA/LPEC/NT/13-5545/A. Dec.2013.
- 1189 [13] J. Brun, C. Reynard-Carette, A. Lyoussi, C. De Vita, M. Carette, M. Muraglia, D. Fourmentel, P. Guimbal and J.F. Villard.
1190 "Comparison of the Thermal Response of Two Calorimetric Cells Dedicated to Nuclear Heating Measurements during Calibration".
1191 Advancements in Nuclear Instrumentation Measurements Methods and their Applications (ANIMMA-2013), Marseille, 23-27 June
1192 2013.
- 1193 [14] "TRIPOLI-4, The Monte Carlo particle transport code of CEA", <http://www.cea.fr/nucleaire/tripoli-4>
- 1194 [15] A. Péron, F. Malouch, C.M. Diop. A. Péron, "Simulation and Comparison of the Calorimeters Measuring the Nuclear Heating in the
1195 OSIRIS Reactor, with the TRIPOLI-4 Monte-Carlo Code", IEEE Transactions on Nuclear Science, Year: 2015 , Volume: 62 , Issue: 3,
1196 Pages: 1218 – 1225
- 1197 [16] H. Carcreff, L. Salmon, and C. Courtaux, "First In-Core Measurement Results Obtained with the Innovative Mobile Calorimeter
1198 CALMOS inside the OSIRIS Material Testing Reactor", IEEE Transactions on Nuclear Science, Vol.61, N°.4, Aug 2014.
- 1199 [17] D. Fourmentel, and coll. "Comparison of Thermal Neutron Flux Measured by ²³⁵U Fission Chamber and Rhodium Self-Powered
1200 Neutron Detector in MTR". IEEE Transactions on Nuclear Science, Vol.61, N°.4, Aug 2014.
- 1201 [18] A. Péron, F. Malouch, and C. Diop. "Improvement of Nuclear Heating Evaluation Inside the Core of the OSIRIS Material Testing
1202 Reactor". 15th International Symposium on Reactor Dosimetry (ISR15), Aix en Provence, May 2014.
- 1203 [19] J. Brun and coll, « influence of thermal conditions on the response of a calorimeter dedicated to nuclear heating measurements », Sensors,
1204 IEEE nov 2014, 1336-1339.
- 1205 [20] E. Brun, F. Damian, C.M. Diop, E. Dumonteil, F.X. Hugot, C. Jouanne, Y.K. Lee, F. Malvagi, A. Mazzolo, O. Petit, J.C. Trama, T.
1206 Visonneau, A. Zoia, Tripoli-4[®], CEA, EDF and AREVA Reference Monte Carlo Code, Annals of Nuclear Energy 82, 151-160 (2015).
- 1207 [21] A. Péron. "Contribution à l'Amélioration des Méthodes d'Evaluation de l'Echauffement Nucléaire dans les Réacteurs Nucléaires à l'aide
1208 du Code Monte Carlo TRIPOLI-4". Rapport CEA-R-6419. Jan, 2016.
- 1209 [22] F. Malouch, E. Brun, F. Damian, F.X. Hugot, F. Lopez, D. Mancusi, O. Petit, A. Zoia, Recent Developments in the Tripoli-4[®] Monte
1210 Carlo Code - Applications to Research Reactors, RRFM/IGORR2016, Berlin, Germany (2016).
- 1211 [23] H. Carcreff, and coll, "First In-Core Simultaneous Measurements of Nuclear Heating and Thermal Neutron Flux obtained with the
1212 Innovative Mobile Calorimeter CALMOS inside the OSIRIS Reactor" IEEE Transactions on Nuclear Science, Vol. 63, N°.5, Oct 2016.

- 1213 [24] "CAST3Mcode", <https://web.archive.org/web/20170913085648/http://www-cast3m.cea.fr/>
- 1214 [25] "euralliage", <https://web.archive.org/web/20170913085547/http://www.euralliage.com/>
- 1215 [26] C.Vargel « propriétés générales de l'aluminium et de ses alliages », techniques de l'ingénieur, ref M4661
- 1216 [27] Rapport d'essai du Laboratoire National d'Essai (LNE). Dossier P164040. Dec 2016.
- 1217 [28] H. Carcreff, L. Salmon,, V. Lepeltier, J.M. Guyot, E. Bouard, "Simultaneous Measurements of Nuclear Heating and Thermal Neutron
- 1218 Flux Obtained with the CALMOS-2 Measurement Device inside the OSIRIS Reactor". Proceedings of ISRD16. Journal of ASTM
- 1219 International, to be published. May, 2017.